

1
2
3
4
5
6
7
8
9
10
11
12
13
14
15
16
17
18
19
20
21
22
23
24
25
26

Technical Note: Rapid assessment of drivers and air quality effects of regional daily changes in air pollutant emissions based on near-real-time techniques

~~**Rapid assessment of drivers and air quality effects of regional daily changes in air pollutant emissions based on near-real-time techniques: A case in Jiangsu Province, China**~~

Chen Gu¹, Yutong Wang^{1,5}, Yuan Ji¹, Lei Zhang^{1,2}, Shuanzhu Sun³, Yuandong Bian¹,
Zimeng Zhang¹, Jiewen Zhu³, Wenxin Zhao¹, Sheng Zhong⁴, Yu Zhao^{1,2*}

¹ State Key Laboratory of Water Pollution Control and Green Resource Recycling and School of Environment, Nanjing University, 163 Xianlin Rd., Nanjing, Jiangsu 210023, China

² Collaborative Innovation Center of Atmospheric Environment and Equipment Technology, CICAET, Nanjing, Jiangsu 210044, China

³ Jiangsu Frontier Electric Power Technology Co., Ltd., 58 Suyuan Ave., Nanjing, Jiangsu 211102, China

⁴ Jiangsu Provincial Environmental Monitoring Center, 100 Zhonghe Rd., Nanjing 210013, China

⁵ Key Laboratory of Formation and Prevention of Urban Air Pollution Complex, Ministry of Ecology and Environment, Shanghai Academy of Environment Sciences, Shanghai 200233, P. R. China

*Corresponding author: Yu Zhao

27 Phone: 86-25-89680650; Email: yuzhao@nju.edu.cn

28

29

30

31 **ABSTRACT**

32 Fast and timely estimation of ~~changing~~ air pollutant emissions is critical for
33 understanding the complex sources of air pollution and supporting air quality
34 improvement, while current ~~regional~~-emission inventory was commonly reported with
35 time lag or coarse temporal resolution. Here we developed a near-real-time approach
36 that calculates the daily emissions of anthropogenic air pollutants, and applied this
37 approach for Jiangsu province, a typical developed region in eastern China. We
38 estimated that the annual total anthropogenic emissions of SO₂, NO_x, primary fine
39 particles (PM_{2.5}), non-methane volatile organic compounds (NMVOCs), and NH₃
40 were 246, 727, 298, 1186, and 377 Gg, respectively, for Jiangsu in 2022. Compared to
41 ~~the available~~ national emission inventory (MEIC), application of the provincial-level
42 daily emission estimates provided better model performance of PM_{2.5} and ozone (O₃)
43 simulation for all ~~the seasons (represented by January, April, July and October)~~
44 ~~involved months~~. The NO_x, SO₂, PM_{2.5}, and NMVOCs emissions in Jiangsu during
45 April-May 2022 (the period of COVID-19 lockdown in Shanghai) were respectively
46 8%, 6%, 6%, and 10% smaller than those in the same period of 2023. Transportation
47 and Industry respectively contributed 89% of NO_x emission reduction and 93% of
48 NMVOCs reduction. Combining with machine learning ~~algorithms~~, moreover, we
49 revealed that the changing agricultural NH₃ emissions dominated the variability of
50 daily PM_{2.5} concentration, and that off-road transportation contributed substantially to
51 variabilities of both PM_{2.5} and O₃ levels. The study proved advantages of
52 incorporation of near-real-time data and machine learning techniques on tracking the
53 fast-changing emissions and detecting the sources of varying air quality.

54 **1. Introduction**

55 Emissions of air pollutants from anthropogenic activity including traffic, industrial
56 plants, and residential and commercial fuel consumption are the main cause of
57 worsened air quality, especially in economically developed regions with dense
58 populations (Sokhi et al., 2022; Zheng et al., 2018). Emission inventory, which
59 contains complete information on magnitude, spatial pattern, and temporal change of
60 air pollutant emissions by sector, is essential for identifying the sources of air
61 pollution and effectiveness of emission controls on air quality through numerical
62 modeling (Zhao et al., 2013; Zhang et al., 2019). Traditionally, “bottom-up”
63 methodology (i.e., the emissions were calculated for the finest source categories and
64 then aggregated to bigger categories) provides robust time series of emission
65 estimates based on national statistics (An et al., 2021; Crippa et al., 2020; Kurokawa
66 et al., 2020). However, these emission estimates were usually reported with a time lag
67 of at least 3-5 years. The delay reflected the time needed to finalize accurate national
68 statistics (e.g., official energy consumption by fuel type) and that needed to collect
69 and process them for compiling emission inventories (Guevara et al., 2023). As a
70 result, in addition to the inherent uncertainties in emission inventories, this delay can
71 introduce extra uncertainty when these inventories are employed in air quality
72 modeling, as they may miss current emission characteristics (Tong et al., 2012). Such
73 limitation can be greatly exacerbated for periods with big and unexpected emission
74 fluctuations, resulting from temporary actions for major events or public health
75 incidents (Huang et al., 2021; Wang et al., 2025).

76 To better track the changing emissions for specific events or incidents (e.g.,
77 COVID-19 pandemic), researchers have developed alternative methods to obtain the
78 near-real-time emission estimates (Gaubert et al., 2021; Schneider et al., 2022). The
79 objective of these efforts is to understand the driving factors of the changing
80 emissions and their impact on air quality. Real-time activity information with high
81 temporal resolution started to be incorporated in the emission estimation, such as the

82 electricity load and generation data by national transmission system operators, the
83 real-time vehicle flows monitored from navigation applications, and the real-time ship
84 navigational information from automatic identification system (AIS) (Liu et al., 2020a;
85 Liu et al., 2020b; Zheng et al., 2021; Huang et al., 2021; Harkins et al., 2021; Guevara
86 et al., 2021). Although limited availability and huge capacity of these data hinder their
87 full use in emission inventory development, there is a big potential in expanding the
88 data source to improve the capability of capturing the fast-changing emissions.

89 Currently, studies have been conducted for carbon dioxides (CO₂) emissions and
90 near-real-time data platforms and products have been developed, particularly for
91 well-identified stationary sources such as fossil fuel combustion plants (BEIS, 2022;
92 CBS, 2024; CITEPA, 2024; Carbon Monitor, 2024). Comparatively, achieving
93 near-real-time estimates is more challenging for air pollutants due to the large
94 complexity and variability of their emission processes. A great variety of air pollutants
95 come from a wide range of sources, containing fuel combustion, industrial processes,
96 on-road and off-road traffic, solvent evaporation, and agricultural activities (Xu et al.,
97 2023; Zheng et al., 2020). The emissions can be greatly influenced by many factors
98 and change a lot. Those factors include the human behavior patterns, operating
99 conditions of plants, improved use of manufacturing and pollution control
100 technologies, and/or meteorological conditions (Liu et al., 2024; Lei et al., 2023;
101 Geng et al., 2024). Given the strong chemical reactivity and short atmospheric
102 lifetime of many air pollutants, there exist complicated relationships between
103 emissions and air quality, emphasizing the importance of tracking the fast-changing
104 emissions (Liu et al., 2020; Zhao et al., 2020a). Therefore, efforts are still in great
105 need to develop effective approach for estimating the near-real-time emissions.

106 For the past years, China has substantially enhanced emission control for industrial
107 (e.g., “ultra-low” emission retrofit for selected non-electrical industries) and
108 residential sources (e.g., promotion of advanced stoves and clean coals during heating
109 seasons). Those measures have clearly reduced emissions of many air pollutants,
110 resulting in a 17.2 µg/m³ decline of fine particle (PM_{2.5}) concentration between 2015

111 and 2020 over the country (Geng et al., 2024). In contrast, the emissions of NO_x and
112 PM_{2.5} from passenger transportation respectively grew by 178% and 152% from 2019
113 to 2022 (Zhang et al., 2023), and the maximum daily 8h mean ozone (MDA8 O₃)
114 concentrations increased 5.8% from 2021 to 2022 for the country (MEE, 2023). The
115 diverse changes in emissions and air quality highlight the necessity to quickly and
116 accurately reveal the drivers of changes in air pollutant emissions and their impact on
117 ambient air quality (Gu et al., 2023). This is particularly important for periods with
118 severe air pollution episodes and unexpected incidents that substantially changed
119 human activities like COVID-19 lockdown, as timely temporary actions to address
120 pollution might be urgently required.

121 Province serves as a crucial role in air quality management in China. Due to
122 difference in economic and energy structure and atmospheric conditions, local
123 governments often implement diverse strategies and actions to reduce regional air
124 pollution. This results in large variability in both emission and air quality changes
125 across different regions. (Liu et al., 2022; Wang et al., 2021). Studies relying on
126 national emission data offer limited guidance in developing emission control
127 measures and assessing their effectiveness in air quality improvement (An et al.,
128 2021). Jiangsu Province, located in the Yangtze River Delta (YRD) in eastern China,
129 is one of most economically developed regions across the country (Supplementary
130 Figure S1). It accounted for 10.2% of the gross domestic product (GDP) in mainland
131 China (ranking the second place in the country), and 8.1%, 12.4% and 11.6% of coal
132 consumption, cement and crude steel production in 2022, respectively (NBS, 2023).
133 Following the implementation of air pollution prevention measures, the PM_{2.5}
134 pollution in Jiangsu has significantly decreased since 2015. However, the
135 development of the petrochemical industry and transportation has led to rapid changes
136 in emissions, making Jiangsu as the province with the highest and fastest growing O₃
137 concentration in YRD in recent years (Zhou et al., 2017; Wang et al., 2022).

138 In this study, therefore, we selected Jiangsu as an example to demonstrate the
139 development of near-real-time emission inventory and its application on rapid

140 assessment of air quality. Based on our previous work that incorporated the best
141 available facility-level information to develop a comprehensive provincial emission
142 inventory (Gu et al., 2023), here we constructed an approach driven by real-time
143 activity data from multiple sources. In this study, “near-real-time” refers to two
144 fundamental aspects. First, the emissions were rapidly estimated based on dynamic
145 activity data, with a minimal delay. It greatly bridged the substantial temporal gap
146 between the occurrence of emissions and the release of official statistical data. Second,
147 it refers to high temporal resolution of the emission data. Unlike previous emission
148 inventories that commonly provided monthly or annual average estimates, the
149 near-real-time approach provided daily emission data and thereby captured the short
150 and temporary perturbations of emissions from anthropogenic activities. The
151 pollutants include SO₂, NO_x, primary PM_{2.5}, NH₃, and non-methane volatile organic
152 compounds (NMVOCs). We then applied the method to obtain the near-real-time
153 emission estimates for 2022-2023, and assessed the driving factors of the short-term
154 emission change during the COVID-19 lockdown period. Finally, we used an Extreme
155 Gradient Boosting (XGBoost) algorithm to explore the relationship between the
156 variability of daily PM_{2.5} and O₃ concentrations and their precursor emissions for
157 2022. The study provides insights for timely design and implementation of air
158 pollution control actions, and can be used for reference for other developed and
159 polluted regions in China and worldwide.

160 **2. Methodology and data**

161 **2.1 Framework of near-real-time emission estimation**

162 Figure 1 shows the methodological framework. In our previous study (Gu et al., 2023),
163 we collected, examined, and integrated most available information on emission
164 sources to enhance the completeness and reliability of the provincial emission
165 inventory. All the information, including raw material and energy consumption,
166 product output, and manufacturing and emission control technologies, played an
167 important role in the estimation of near real-time emissions. The specific methods by

168 sector are described in Section 2.2. To ensure the robustness of the near-real-time
169 activity data (e.g., traffic indices and CEMS records), a rigorous data quality control
170 protocol was implemented to handle missing values and outliers. Obvious anomalies,
171 defined as values exceeding three standard deviations from the 7-day moving average,
172 were screened and removed. For short-term data gaps (1-2 days), linear interpolation
173 was applied. For longer continuous missing periods (≥ 3 days), missing values were
174 gap-filled using the historical average of the same day-of-week in the adjacent weeks,
175 adjusted by the regional sector-specific variability.

176 Furthermore, we improved the spatial distribution of air pollutant emissions. Point
177 sources of power and industrial enterprises were allocated based on their latitudes and
178 longitudes. We further utilized Point of Interest (POI) data from Gaode Map
179 (<https://lbs.amap.com/>, last visited on October 2025) to obtain changes on
180 road/waterway networks, land use, and building footprints. The spatial information is
181 commonly updated every 2-3 months. The use of updated POI data greatly reduced
182 the error of spatial allocation of emissions that may result from the delayed
183 information from the constant spatial proxies (Wang et al., 2017).

184 **2.2 Near-real-time daily emission estimation by sector**

185 This section describes the methods for estimating near-real-time daily emissions for
186 2022 and 2023. Six major sectors were included (Power, Industrial plant, Vehicles
187 (On-road transportation), Off-road machinery, Residential, and Agriculture), covering
188 most anthropogenic activities. Road and construction site dusts were not contained.

189 **Power plant** Previously we developed a method of applying online measurement data
190 from the continuous emission monitoring systems (CEMS,
191 <http://218.94.78.61:8080/newPub/web/home.htm>, last visited on October 2025) for
192 emission estimation at the unit/plant level (Zhang et al., 2019). With this basis, we
193 have improved the emission estimation method to enable the stable and continuous
194 acquisition of near-real-time emission data lagged by one month. For the small
195 number of power-generating units without CEMS data, we assumed that their

196 pollutant concentrations in the flue gas were at the average level of units with similar
 197 installed capacity (Tang et al., 2019). The emissions were calculated based on the
 198 mean hourly flue gas concentration of air pollutant obtained from CEMS and the
 199 theoretical flue gas volume of each unit/plant:

$$200 \quad E_{i,j,day} = C_{i,j,month} \times AL_{j,month} \times V_{j,m}^0 \times P_{i,j,m,day} \quad (1)$$

$$201 \quad AL_j = F_m / R_m \quad (2)$$

202 where E is the emission of air pollutant; i, j and m indicate the specific pollutant
 203 species, individual power plant or unit, and fuel type, respectively; C is the monthly
 204 average concentration in the flue gas; AL is the activity level (here monthly coal
 205 consumption); F is the monthly electricity generation for various fuels, as reported by
 206 NBS (2023); R is the fuel consumption rate for power generation, taken from Tong et
 207 al. (2021), V^0 is the theoretical volume of flue gas produced per unit of fuel
 208 consumption (Zhao et al., 2010); P is the temporal profile of emissions (the daily to
 209 monthly emission ratio), based on the hourly pollutant concentrations and volume of
 210 flue gas for the month and specific day.

211 **Industrial plant** With its gradually expanding penetration, CEMS has become able to
 212 support near-real-time emission estimation for industrial plants (Tang et al., 2022; Bo
 213 et al., 2021). Given its varying coverage across sectors, we have developed a method
 214 that can stably estimate the near-real-time emissions at the plant level with a lag of
 215 one month. This method classifies industrial plants into three categories based on their
 216 CEMS coverage, as described below.

217 (1) Industrial plants with CEMS information. The method is similar to power plants:

$$218 \quad E_{i,j,day} = C_{i,j,month} \times AL_{j,month} \times V_{i,j,k}^0 \times P_{i,j,m,day} \quad (3)$$

219 where k denotes the industrial sector; AL is the activity level (here represents monthly
 220 product output) as reported by NBS (2023), and V^0 is the theoretical volume of flue
 221 gas produced per unit of product output, which can be found in the technical
 222 specifications for the application of emission permits (MEE, 2021).

223 (2) Industrial plants without CEMS while it was equipped at some plants within the
 224 same sector. Sector-level emission factors (emissions per unit of activity level, EF)

225 were calculated using CEMS data from other plants. Monthly emissions were
 226 estimated based on the sector-level EF and monthly product output from official
 227 environmental statistics. The near-real-time daily emissions were then generated
 228 according to the temporal profile of emissions (P) obtained from CEMS installed in
 229 other available plants in the sector.

$$230 \quad E_{i,j,day} = AL_{j,month} \times EF_{i,k} \times P_{i,j,m,day} \quad (4)$$

$$231 \quad EF_{i,k} = E_{i,k,month} / AL_{k,month} \quad (5)$$

232 where $EF_{i,k}$ is the sector-average emission factor for plants with CEMS for sector k ,
 233 $E_{i,k}$ and AL_k are the total emissions from industrial plants with CEMS and their
 234 product output, respectively.

235 (3) Industrial sectors without CEMS data. Emissions were principally calculated
 236 based on activity level and emission factor. The activity data were derived based on
 237 monthly official statistics reported by NBS (2023). In addition, we analyzed the
 238 historical emission source data to trace the evolution of manufacturing and emission
 239 control technologies for various sectors, and the emission factors could be calculated
 240 for near-real-time emission estimations:

$$241 \quad E_{i,day} = AL_{month} \times EF_{i,k} \times P_{i,m,day} \quad (6)$$

242 where EF represents the emission factor based on the technological evolution of the
 243 plant, P is the temporal profile of emissions, based on the fraction of daily electricity
 244 load out of the monthly total for specific sector.

245 **Vehicles (On-road transportation)** Daily vehicular emissions were estimated
 246 utilizing the International Vehicle Emissions model (IVE) combined with the Gaode
 247 live congestion index (Zhou et al., 2019; Kholod et al., 2016). The level of traffic
 248 congestion was indicated by the additional time incurred during a trip under congested
 249 conditions, expressed as a percentage relative to uncongested conditions (Huo et al.,
 250 2022). The Gaode congestion index is available for over 350 cities in China, with a
 251 temporal resolution of 5 minutes (<https://report.amap.com/index.do>, last visited on
 252 October 2025). By integrating the congestion index with a Greenshield's traffic
 253 density model (Yang et al., 2019), we estimated the traffic volume which serves as a

254 temporal allocation factor to calculate the daily emissions. This approach assumes that
 255 vehicular activity data (e.g., mileage and fuel consumption) are accessible, albeit
 256 typically with a lag in reporting, as such information is usually provided on an annual
 257 basis. Consequently, the near-real-time emissions can be estimated based on the daily
 258 variations of congested index and EFs compared to the previous year (Eq. 7):

$$259 \quad E_{i,m,day} = \frac{(I_{day,year-1}) \times I_{day,(year-1)}^2 \times EF_{i,m,day,year}}{(I_{day,(year-1)}-1) \times I_{day,year}^2 \times EF_{i,m,day,(year-1)}} \quad (7)$$

260 In Equation (7), EF represents the emission factor calculated by the IVE model. The
 261 input parameters of IVE, such as vehicle population by type, registration dates, fuel
 262 types, and emission standards, can be obtained from the transportation management
 263 departments of individual cities. These historical data can be extrapolated to the
 264 present date utilizing the vehicle survival curve, thereby bridging any gaps in the
 265 current information (Sun et al., 2020). Because official high-frequency traffic activity
 266 data are unavailable in near-real-time, we introduced I , the Gaode traffic congestion
 267 index, as a dynamic activity scaling factor. This index reflects the comprehensive
 268 traffic volume and operational status of the overall road network, allowing us to
 269 dynamically scale the baseline emissions into daily-scale trajectories. The index
 270 serves as a generalized proxy for total road network activity, and the same scaling
 271 factor was applied uniformly for all vehicle types. Although different temporal
 272 operational patterns might exist for various vehicle types (e.g., larger volume for
 273 trucks during nighttime or on specific freight corridors), obtaining the near-real-time
 274 activity information by vehicle type remains a challenge at the provincial level in
 275 China. The baseline EF for vehicles in Equation 7 were derived using the IVE model,
 276 which comprehensively accounts for the influences of complex driving conditions,
 277 including vehicle speed and engine load. However, continuous recalculation of
 278 real-time and speed-dependent EFs on a daily, province-wide scale is computationally
 279 intensive and remains as a challenge. For the near-real-time estimation of traffic
 280 emissions, therefore, the EFs were treated as baseline constants for 2022, and we
 281 predominantly focused on the dynamic adjustment of activity levels and treated them
 282 as the primary driving factor for the daily emission fluctuations.

283 **Off-road Transportation** Off-road transportation was divided into five categories:
284 construction machinery, agricultural machinery, marine, railway, and aviation.
285 Emissions from construction machinery were estimated based on assumed daily
286 utilization rates derived from the operating rates of construction sites (Shen et al.,
287 2023; Huang et al., 2021). The daily usage of agricultural machinery was assumed to
288 correlate with the application of nitrogen fertilizers from agricultural sources (see the
289 description of agriculture as below). Emissions from railway, marine and aviation
290 sources were estimated using data from passenger/cargo turnover, individual ports and
291 commercial flights, respectively. These data were obtained from the China
292 Entrepreneur Investment Club (CEIC) (<https://www.ceicdata.com.cn>, last visited on
293 October 2025), Marine Traffic (<http://www.marinetraffic.com>, last visited on October
294 2025) and Flightradar24 databases (<http://www.flightradar24.com>, last visited on
295 October 2025) (Huo et al., 2022; Liu et al., 2020a).

296 **Residential sources** We followed Shao et al. (2023) and developed a Bayesian
297 hierarchical model to estimate daily heating energy consumption by fuel type, based
298 on two primary factors influencing residential energy consumption: temperature and
299 GDP. The daily temperature data were taken from ERA5 products provided by the
300 European Centre for Medium-Range Weather Forecasts (ECMWF)
301 (<https://cds.climate.copernicus.eu>, last visited on October 2025), while GDP from the
302 national statistics published quarterly by the National Bureau of Statistics
303 (<http://www.stats.gov.cn/>, last visited on October 2025). For the months without GDP
304 data, we assumed a linear relationship between GDP and the nighttime light index (Xu
305 et al., 2024), and applied the National Polar-orbiting Partnership Visible Infrared
306 Imaging Radiometer Suite (NPP-VIIRS, <https://www.earthdata.nasa.gov/>, last visited
307 on October 2025) provided by National Aeronautics and Space Administration
308 (NASA) to extrapolate the GDP for those months. We applied the gridded population
309 dataset (1km×1km) released by a database of the Chinese Academy of Sciences
310 (<https://www.resdc.cn/Default.aspx>, last visited on October 2025) for 2020. To
311 account for the effect of large-scale population migration, we integrated the

312 Population Migration Index (PMI) developed by Baidu (<https://qianxi.baidu.com/#/>,
313 last visited on October 2025). This index calculates the proportion of incoming
314 migrants relative to the local population.

315 **Agriculture** NH₃ emissions from fertilizer use can be largely influenced by
316 meteorological conditions, soil environment, and farming practices. In our previous
317 study, we quantified NH₃ emissions using dynamic EFs associated with those factors
318 (Zhao et al., 2020b). In this study, we expanded the methodology and estimated NH₃
319 emissions by using daily EFs. Regarding the baseline activity data for NH₃
320 estimations, the information was systematically derived from official statistics. For
321 livestock and poultry breeding, we utilized the year-end stock. For synthetic fertilizers,
322 the application amount was calculated as the product of the city-level sown area of
323 cropland and the provincial application rate per unit area obtained from national
324 investigations. To convert these annual totals into dynamic near-real-time estimations,
325 we integrated the temporal allocation of activity data with real-time meteorological
326 conditions. Based on the regional farming database from the Ministry of Agriculture,
327 we tracked the specific growing seasons of major crop types to determine the exact
328 timing of basal dressing and top dressing. By combining the farming cycles with
329 meteorological conditions and high-resolution soil pH databases, we generated the
330 spatiotemporal pattern of NH₃ emissions.

331 **2.3 Air quality modeling**

332 To evaluate the near-real-time emission estimate, we used the Community Multiscale
333 Air Quality (CMAQ v5.1) model developed by US Environmental Protection Agency
334 (<https://www.epa.gov/cmaq>, last visited on October 2025), to simulate the PM_{2.5} and
335 O₃ concentrations in Jiangsu. Four months (January, April, July, and October) in 2022
336 were selected as the simulation periods, with a spin-up time of 7 days for each month
337 to reduce the impact of the initial condition on the simulation. As shown in
338 Supplementary Figure S1, three nested domains (D1, D2, and D3) were applied with
339 the horizontal resolutions at 27, 9, and 3 km, respectively, and the most inner D3

340 covered Jiangsu and parts of the YRD region including Shanghai, northern Zhejiang,
341 and eastern Anhui. The Multi-resolution emission inventory of China (MEIC, [http://](http://meicmodel.org.cn/)
342 <http://meicmodel.org.cn/>, last visited on October 2025) was applied for D1, D2, and
343 the regions out of Jiangsu in D3 (Zheng et al., 2018), and the provincial-level
344 near-real-time emission estimate was applied for Jiangsu in D3. The Carbon Bond
345 Mechanism (CB05) and AERO5 mechanisms were used for the gas-phase chemistry
346 and aerosol module, respectively.

347 The meteorological field for the CMAQ was obtained from the Weather Research and
348 Forecasting model (WRF v3.4, <https://www.mmm.ucar.edu/models/wrf>, last visited on
349 October 2025). Meteorological initial and boundary conditions were obtained from
350 the National Centers for Environmental Prediction (NCEP,
351 <https://psl.noaa.gov/data/reanalysis/reanalysis.shtml>, last visited on October 2025)
352 datasets. Ground observations at 3-h intervals were downloaded from National
353 Climatic Data Center (NCDC, <ftp://ftp.ncdc.noaa.gov/pub/data/noaa/isd-lite/>, last
354 visited on October 2025). Statistical indicators including bias, index of agreement
355 (IOA), and root mean squared error (RMSE) were used to evaluate the WRF
356 performance (Gu et al., 2023). The discrepancies between simulations and ground
357 observations were within an acceptable range (Supplementary Table S1).

358 We collected ground observation data of hourly PM_{2.5} and O₃ concentrations at the
359 110 state-operating air quality monitoring stations within Jiangsu
360 (<https://data.epmap.org/page/index>, see the station locations in Figure S1, last visited
361 on October 2025). Correlation coefficients (R), normalized mean bias (NMB) and
362 normalized mean errors (NME) between observation and simulation for each month
363 were calculated to evaluate the performance of CMAQ modeling.

364 We further compared the modeling performance using the provincial-level
365 near-real-time emission estimates in D3 with that based on MEIC. Since MEIC was
366 currently available till 2020, direct application of MEIC introduce bias from the
367 discrepancy in annual total emissions for different years. To avoid this, we adjusted
368 the annual total emissions of various species in MEIC (for Jiangsu 2020) to perfectly
369 match those of our near-real-time estimates (for Jiangsu 2022), and kept the

370 spatiotemporal distribution of emissions unchanged (referred as “MEIC-revision”).
371 The treatment ensured that any improvement in modeling performance with the
372 near-real-time emission estimate resulted from its optimized spatiotemporal pattern of
373 emissions rather than the total levels.

374 **2.4 Removing meteorological influence on PM_{2.5} and O₃ concentrations**

375 To explore the influence of anthropogenic emission changes on the variability of
376 PM_{2.5} and O₃ levels in 2022, we removed the impact of varying meteorological
377 conditions by employing a stepwise multiple linear regression (MLR) model (Li et al.,
378 2021). The surface daily concentrations of O₃ and PM_{2.5} were taken from the Tracking
379 Air Pollution in China (TAP, <http://tapdata.org.cn/>, last visited on October 2025) with
380 a horizontal resolution of 1 km×1 km (Geng et al., 2021). We incorporated nine
381 meteorological variables from the ERA5 database at a resolution of 0.25°×0.25°,
382 considered as the potential covariates for O₃ and PM_{2.5}. They were 10-meter zonal and
383 meridional wind speeds, temperature, boundary layer height, sea level pressure, cloud
384 cover, precipitation, relative humidity, and dew point temperature. These variables
385 were then scaled to a 3km×3km grid system by bilinear interpolation. To prevent
386 overfitting, we conducted MLR with the three most influential meteorological
387 parameters to estimate the variability of daily PM_{2.5} and maximum daily 8-hour
388 average (MDA8) O₃ concentration for each grid cell. Anomaly (the difference
389 between the raw data and the moving average of 30 days around) of air pollutant
390 concentrations and meteorological factors were used in the model, to exclude the
391 effect of monthly variability. Residuals that cannot be explained by the meteorological
392 variables were assumed to be attributed to anthropogenic emission changes (Li et al.,
393 2020). The results could be interpreted as the sensitivity of air pollutant concentration
394 to the daily emission anomalies from the annual average value.

395 To evaluate the MLR performance, we collected daily PM_{2.5} and O₃ concentrations at
396 the above-mentioned 110 air quality monitoring stations in Jiangsu (Figure S1), and
397 the R and NMB between observation and MLR were calculated.

398 **2.5 Examining the response of MDA8 O₃ and PM_{2.5} concentration to changing**
399 **daily emissions**

400 **2.5.1 XGBoost model**

401 XGBoost model is an advanced and scalable machine learning framework based on
402 gradient-boosted decision trees, widely recognized for its efficiency in handling
403 structured data and modeling complex nonlinear relationships (Requia et al., 2020;
404 Wang et al., 2023). XGBoost excels at processing high-dimensional spatiotemporal
405 datasets, such as gridded emission inventories, by effectively capturing interactions
406 among heterogeneous emission sources and temporal dependencies. Moreover, the
407 inherent interpretability features facilitate seamless integration with explainable AI
408 tools (e.g., SHapley Additive exPlanations (SHAP) to quantify the marginal
409 contribution of each input feature to individual model predictions), enabling rigorous
410 attribution analysis of air pollutant concentration variability (Zhao et al., 2025). To
411 overcome the traditional “black box” limitation of tree-based machine learning
412 models, we utilized the SHAP algorithm to interpret the XGBoost outputs. Based on
413 the algorithm, we were able to explicitly attribute the day-to-day variations in ambient
414 pollutant concentrations to precursor emission changes from specific sectors, thereby
415 drawing physically meaningful and conclusions.

416 The SHAP value is calculated with following equation:

417
$$y_i = y_{base} + f(X_{i,1}) + f(X_{i,2}) + \dots + f(X_{i,n}) \quad (8)$$

418 where y_i is the predicted value of the model for the i th sample; $f(X_{i,n})$ is the
419 contribution of the n th eigenvalue in the i th sample to the final predicted value, with
420 positive or negative representing that the eigenvalue makes the predicted value
421 increase or decrease; and y_{base} is the baseline value of the predicted outputs for all
422 types of predictions, representing the average prediction results for each category
423 without the influence of any eigenvalue.

424 **2.5.2 Anthropogenic effects on PM_{2.5} and MDA8 O₃ variability**

425 The XGBoost-SHAP modeling framework was implemented at the horizontal
426 resolution of 3km×3km to capture the emission-concentration relationship. XGBoost
427 regression models were independently trained for each grid cell. January and July
428 were selected as typical months for ambient PM_{2.5} and O₃, respectively. Daily time
429 series of 20 pollutant-sector combinations (4 pollutant (SO₂, NO_x, NMVOCs, PM_{2.5})
430 × 5 sectors (Power, Industry, On-road (Vehicles), Off-road, Residential) except for
431 tiny On-road SO₂, and agricultural NH₃,) were set as predictors, and
432 anthropogenic-driven variability of PM_{2.5} or O₃ concentrations as target variables.
433 Similarly, the emission inputs were treated as anomaly (the difference between the
434 current day's emissions and the moving average of 30 days around). A 10-fold
435 cross-validation was applied (80% training and 20% testing), and the bias and
436 correlation coefficient (R) were calculated to evaluate the model performance (Xiao et
437 al., 2018).

438 SHAP values were calculated for each emission feature using the tree explainer
439 algorithm, quantifying contributions of pollutant-sector combinations to variability of
440 daily anthropogenic-driven concentrations. Note that SHAP values represented the
441 deviation of individual predictions from the baseline expectation. Positive values
442 indicated emission features that elevated pollutant concentrations above the baseline,
443 while negative values indicated features that reduced concentrations below the
444 baseline. Aggregation of daily SHAP values for various pollutant-sector combinations
445 produced the daily-level contribution of total anthropogenic emissions to the changing
446 ambient concentration, and the daily-level contributions could then be aggregated to
447 the monthly level.

448 **3. Results and discussions**

449 **3.1 Anthropogenic air pollutant emissions**

450 **3.1.1 Total air pollutant emissions in 2022**

451 The total anthropogenic emissions of SO₂, NO_x, PM_{2.5}, NMVOCs, and NH₃ in
452 Jiangsu for 2022 were estimated at 246, 727, 298, 1186, and 377 Gg (Supplementary
453 Figure S2), which were respectively reduced by 17%, 33%, 18%, 7%, and 11%
454 compared with those in 2019 (Gu et al., 2023). Note the emissions for multiple years
455 (2015, 2019, and 2022) were estimated with a consistent methodological framework
456 to make reasonable interannual comparison. Our estimates indicated that the reduction
457 rate of SO₂ emissions was much lower between 2019 and 2022 than that at 53%
458 between 2015 and 2019. In particular, the emissions from the power sector were
459 estimated to decline only 7% during 2019-2022. The result confirmed that the
460 abatement of SO₂ emissions have been clearly decelerated following the full
461 implementation of ultra-low emission retrofits, suggesting that the potential of further
462 reduction of SO₂ emissions for power sectors has become more limited. More energy
463 structure adjustment instead of end-of-pipe controls is needed for the sector.

464 In contrast to SO₂, the emissions of NO_x and PM_{2.5} were estimated to decline faster
465 during 2019-2022 than 2015-2019. Industrial sectors contributed largely to these
466 reductions, with the emission declining 27% and 22% for NO_x and PM_{2.5},
467 respectively (Figure S2). These reductions reflected expansion of intensified pollution
468 control policies from power to other sectors, particularly the ultra-low emission
469 standards implemented for steel (2019) and cement industries (2020)
470 (<https://sthjt.jiangsu.gov.cn/>, last visited on October 2025). By 2022, Jiangsu province
471 had implemented ultra-low emission retrofits in over 80% of iron & steel enterprises
472 and approximately 60% of cement clinker production lines (DEE, 2023). However,
473 slower progress of emission controls in coking, glass, and chemical industries
474 highlighted substantial emission reduction potential in these non-electrical industrial
475 sectors. Meanwhile, the NO_x emissions of transportation were estimated to decline by
476 41% from 2019 levels (53% for light-duty gasoline vehicles), driven mainly by the
477 nationwide implementation of China VI vehicle emission standard and increasing
478 penetration of renewable energy vehicles.

479 NMVOCs, as critical precursors of both secondary PM_{2.5} and O₃ formation, exhibited

480 a slower decline in emissions and have emerged as the priority of emission controls in
481 Jiangsu (Figure S2). Industrial activities dominate NMVOCs emissions in Jiangsu,
482 contributing 68% of the provincial total emissions. It resulted from the heavy
483 dependence of the province on chemical industries. For example, the province
484 accounted for over 40% of national pesticide active ingredient and dye production.
485 Notably, more than 60% of small-scale chemical enterprises persisted in utilizing
486 solvent-based coatings, inks, and adhesives with high-VOCs content (Simayi et al.,
487 2022; Hu et al., 2024). Furthermore, recent expansions in solvent consumption and
488 chemical output within large-scale enterprises along the Yangtze River have largely
489 offset the emission reductions through improvement of manufacturing and pollution
490 control technologies (Li et al., 2019). Consequently, intensified emission controls
491 should be urgently required for targeting key industrial sectors and critical regions for
492 NMVOCs reduction. Agricultural NH₃ emissions in Jiangsu have experienced a
493 decline of 14% during 2019-2022, primarily attributed to reduced nitrogen fertilizer
494 usage. However, the absence of effective NH₃ control measures prevented further
495 substantial reduction of emissions for the sector (Zhou et al., 2023; Zhao et al., 2022).

496 **3.1.2 Daily emission variability for air pollutants in 2022**

497 Figure 2 show the daily variability of total and sectoral emissions of various pollutants
498 (SO₂, NO_x, PM_{2.5}, NMVOCs, and NH₃) in 2022, respectively (the time series of
499 emissions (NO_x as an example) for all the involved source categories are provided in
500 Supplementary Figure S3). The results revealed distinct seasonal emission patterns of
501 air pollutants driven by anthropogenic activities and/or meteorological conditions.

502 The emissions of SO₂ and primary PM_{2.5} followed the seasonal patterns of fossil
503 energy consumption (Yun et al., 2021), with clear peaks in winter (from December to
504 February) associated with the substantial coal combustion for residential heating and
505 elevated industrial energy demand (Geng et al., 2021; Zhan et al., 2023). Regarding
506 NO_x, transportation has become the primary contributor to the emissions along with
507 improved emission controls from the power and industrial sectors. Following the

508 lifting of COVID-19 lockdown since June 2022, moreover, residents exhibited a
509 strong desire to travel, which enhanced the emissions from transportation. Compared
510 to the spring (from March to May), NO_x emissions from transportation increased 12%
511 during the summer (from June to August), consistent with the elevated population
512 mobility (Supplementary Figure S4). Additionally, the NO_x emission peak in March
513 reflected the resumption of industrial production and construction activities after the
514 Chinese New Year. The area of construction for residential and commercial buildings
515 increased 56% from February to March, with these activities heavily dependent on
516 diesel-powered machinery (Yang et al., 2015; Cliff et al., 2023). The NMVOCs
517 emissions were the largest in summer. Enhanced volatilization of solvents and
518 industrial chemicals by the warmer temperatures resulted in a 22% growth of summer
519 emissions compared to spring. Similar to NO_x, the NMVOCs emissions in March
520 rebounded with a 17% growth compared to February, reflecting the resumption of
521 coating, printing, and petrochemical industries. For NH₃, the highest emissions in
522 March and September were predominantly driven by the intensive spring sowing and
523 autumn farming seasons. In contrast, although the total fertilizer amount decreased in
524 summer (mainly limited to top dressing for specific crops like paddy rice), the high
525 temperature in summer together with top dressing greatly elevated the NH₃
526 volatilization rates, resulting in peak emission factors that kept the emissions at a high
527 level.

528 Notably, the province has made great efforts on reducing emissions during the period
529 with heavy pollution weather (DEE, 2022). The restriction measures included
530 alternating operations of energy-intensive industrial plants, such as cement, steel, and
531 glass production, in order to reduce the total production level and energy consumption
532 during the period. Furthermore, industrial parks were required to temporarily shut
533 down or to reduce the load of coal-fired boilers to mitigate regional precursor
534 emissions under the unfavorable meteorological conditions. Compared to August
535 2022, mandatory restrictions on coal-fired boilers and industrial plants for September
536 resulted in an 11% reduction of coal consumption for major industrial sectors, leading

537 to a decline of 7%, 10%, 15%, and 12% for anthropogenic emissions of SO₂, NO_x,
538 PM_{2.5}, and NMVOCs, respectively. This demonstrated the effectiveness of pollution
539 control measures conducted by the government on counteracting pollution episodes
540 around August and September, despite persistent meteorological challenges (Wang et
541 al., 2023). However, subsequent emission rebounds in winter for SO₂ (+24%
542 compared with those in Autumn) and PM_{2.5} emissions (+19%) underscored the
543 limitation of seasonal control strategies for combustion-derived pollutants,
544 emphasizing the imperative for clean energy promotion to achieve sustainable
545 emission abatement.

546 In April 2022, a great reduction in air pollutant emissions was estimated. Compared
547 with March, the emissions of SO₂, NO_x, PM_{2.5}, and NMVOCs decreased by 11%, 8%,
548 6%, and 12% respectively. This abrupt decline was temporally associated with the
549 COVID-19 induced lockdown implemented in Shanghai (March 28-June 1, 2022).
550 The lockdown substantially disrupted industrial production, transportation activities,
551 and daily routines in neighboring Jiangsu Province. The results showed that
552 short-term public health incidents exerted profound impact on air pollutant emissions
553 (Zhang et al., 2024; Ma et al., 2023).

554 **3.1.3 High-resolution maps of air pollutant emissions**

555 Based on the real-time geospatial information from the POI system (e.g., quarterly
556 updated road networks, land use types, and monthly revised construction sites), we
557 achieved the evolving spatial pattern of daily air pollutant emissions with a horizontal
558 resolution of 3 km×3 km. Figure 3 presents the spatial distribution of daily average
559 emissions of major sectors in Jiangsu Province for 2022. We selected NO_x as an
560 example to illustrate the sector heterogeneity. The NO_x emissions from power,
561 industrial, vehicle, off-road transportation and residential sources in Jiangsu were
562 calculated at 144, 109, 247, 183 and 45 Gg respectively. Aviation emissions (less than
563 1% of total NO_x) were excluded due to their tiny contribution to the total emissions.

564 The spatial pattern of emissions was closely associated with corresponding

565 anthropogenic activities. Agricultural machinery emissions were predominantly
566 located in northern agricultural zones and coastal areas, correlating with the
567 spatiotemporal distribution of farming activities. In contrast, emissions from other
568 sources were more concentrated in the southern cities, especially along the Yangtze
569 River with the most abundant power and industrial plants. The NO_x emissions from
570 five cities in southern Jiangsu (Nanjing, Suzhou, Wuxi, Changzhou, Zhenjiang)
571 accounted for 59% and 63% of provincial power and industrial emissions,
572 respectively. On-road transportation emissions demonstrated a strong dependence on
573 the road network. Nanjing and Xuzhou, as critical national railway transportation hubs,
574 contributed 24% and 13% of provincial NO_x emissions from railways (Wang et al.,
575 2016). In addition, Suzhou contributed 29% of provincial marine emissions, attributed
576 to its pivotal role in Yangtze River Delta inland waterway logistics (Shen et al., 2021).
577 Unsurprisingly, the residential NO_x emissions were closely correlated with the
578 population density.

579 **3.1.4 Assessment of monthly variability**

580 Figure 4 compares the monthly distributions of SO₂, NO_x, and PM_{2.5} emissions
581 estimated in this study with those in MEIC, as well as those of provincial averages of
582 ambient concentrations of corresponding species obtained from the state-operating
583 observation sites in Jiangsu. Due to the unavailability of MEIC for the year 2022, we
584 used the result for 2020 instead.

585 For SO₂ (Figure 4a) and PM_{2.5} (Figure 4e), similar monthly variation patterns were
586 found between emissions and observed concentrations in Jiangsu. The near-real-time
587 emission estimates effectively captured the short-term fluctuations in anthropogenic
588 activities, including the abrupt reduction in April associated with the COVID-19
589 lockdown and the seasonal change from the temporary pollution control measures in
590 autumn. While ambient concentrations were influenced by meteorology and
591 secondary formation as well, the relatively long atmospheric lifetimes of SO₂ and
592 PM_{2.5} (typically several days) allow them to reflect the impact of primary emission

593 variations. These results partly justified the capability of the approach to track the
594 effect of changing anthropogenic activities on air pollutant emissions. In contrast, the
595 highly reactive nature and shorter atmospheric lifetime of NO_x resulted in a
596 decoupling between its emissions and ambient concentrations. We found contrary
597 monthly distributions between NO_x emissions and the observed NO₂ concentrations
598 (Figure 4c). The largest emissions were estimated in summer months but the lowest
599 concentrations were observed for the same months across the year. This inconsistency
600 likely resulted from the following factors. Increased transportation activity in summer,
601 particularly mobility rebound after lockdown, elevated NO_x emissions. Meanwhile,
602 NO₂ was substantially consumed for O₃ formation through rapid photochemical
603 reactions under the intense solar radiation and high temperatures, and its atmospheric
604 lifetime was reduced to merely a few hours. In winter, there was more NO_x
605 accumulation in the atmosphere with weaker photochemical reactions and reduced
606 boundary layer heights (Ding et al., 2015; Wang et al., 2012).

607 Similar monthly distribution of emissions were found for the national (MEIC) and
608 provincial emission estimates (this work), implying regular patterns of monthly
609 anthropogenic activities could be captured by both inventories. Nevertheless,
610 disparities existed in the overall emission totals and sector distributions between the
611 two inventories. For instance, the contributions of industry to provincial emissions of
612 SO₂ and NO_x were estimated at 45% and 15% in this work, greatly different from the
613 MEIC estimation at 72% and 41%, respectively. These discrepancies might be
614 attributed to that the national inventory (MEIC) for 2020 has not yet fully included the
615 information of emission control technology upgrades (e.g., ultra-low emission
616 retrofits) in the industrial sector. Taking the sintering process in the steel industry as
617 an example, our facility-level estimations indicated that the average emission factors
618 for SO₂, NO_x, and PM_{2.5} were 0.143 kg/t, 0.228 kg/t, and 0.037 kg/t, respectively,
619 much lower than the recommended values of 1.34 kg/t, 0.55 kg/t, and 2.52 kg/t from
620 the guidelines for development of national emission inventory (He et al., 2018).

621 Substantial discrepancies were revealed for off-road transportation of SO₂ emissions.

622 The provincial SO₂ emission estimate from marine (12,877 Mg/yr) were almost three
623 times of that by MEIC (4,690 Mg/yr). As a major freight hub in the eastern coastal
624 region of the country, Jiangsu Province played a pivotal role in marine transportation,
625 and approximately 60% of vessels utilized heavy oil with high-sulfur content as fuel
626 (Dong et al., 2025). Application of national average EFs for the sector might lead to
627 underestimation in emissions. Furthermore, the national inventory ignored the
628 emissions from passing vessels at ports. Inclusion of such vessels would increase the
629 SO₂ emissions in the Yangtze River Delta region by a factor of 2.3 (Zhang et al.,
630 2017). As power and industrial sectors have gradually completed ultra-low emission
631 retrofits, marine emissions with less stringent controls may become more important in
632 the future, requiring greater efforts on fuel quality improvement and stricter emission
633 controls.

634 **3.2 Impacts of short-term lockdown on changes in emissions**

635 From March 28 to June 1 in 2022, Shanghai, the largest megacity in YRD and the
636 national center of economy, finance, manufacturing, and maritime trade in China,
637 implemented stringent COVID-19 lockdown measures that suspended intercity
638 mobility and industrial production and kept only essential logistics. This
639 unprecedented lockdown not only disrupted social and economic activities of
640 Shanghai, but also brought substantial effects for neighboring regions. Jiangsu
641 Province, a highly industrialized region adjacent to Shanghai, experienced severe
642 disruptions across service sectors, manufacturing supply chains, and maritime
643 logistics, resulting in substantial declines in energy consumption, industrial output,
644 and transportation activities. To further quantify the lockdown effect on air pollutant
645 emissions, we conducted a comparative analysis between two periods: the
646 lockdown-affected period (April-May 2022) and the post-pandemic period, the same
647 months one year later (April-May 2023).

648 The first column of Figure 5 (a1, b1, c1, d1) illustrates the variability in daily
649 emissions of NO_x, SO₂, PM_{2.5}, and NMVOCs in Jiangsu during April-May 2022

650 (lockdown period) versus 2023 (recovery period), as well as the difference between
651 the two periods. The emission differences (calculated as the relative change compared
652 to the 2023 level) reached 8%, 6%, 6%, and 10% for these air pollutants, respectively.
653 The most substantial decline in pollutant emissions occurred in April 2022, with a
654 gradually diminishing difference in May. However, the emissions by the end of May
655 2022 did not reach the level of recovery period in May 2023, reflecting the effect of
656 temporary measures on reducing economic activities even after the lifting of the
657 lockdown. The full economy recovery was delayed until 2023 when pandemic
658 restrictions were completely lifted (Li et al., 2023).

659 The second and third columns of Figure 5 (a2-d2 and a3-d3) illustrate the
660 contributions of various pollution source categories to the differences in emissions
661 between April-May of 2022 and 2023. Agricultural production remained basically
662 unaffected by the pandemic, thus the emission changes from agricultural machinery
663 were not included. The total reduction in NO_x emissions was 9,970 Mg,
664 predominantly attributed to transportation sources. The sector contributed to over 70%
665 of the emission reduction, including on-road transportation (15%), construction
666 machinery (27%), marine (19%), railway (5%), and aviation (4%). This result is
667 consistent with the findings on the effect of the 2020 COVID-19 lockdown (Lv et al.,
668 2020; Zhao et al., 2020a). However, there was a slight rebound in motor vehicle
669 emissions in May, which could be associated with basic everyday living and working
670 needs. Notably, construction machinery and marine were more affected by the
671 lockdown, attributable to construction material shortages (39% fewer of constructing
672 and building activities) and disrupted inland waterway logistics (20% less of port
673 throughput). Compared with transportation, the reduction of NO_x emissions from the
674 power (1,955 Mg) and the industrial sector (1,202 Mg) were smaller. The decline in
675 industrial electricity demand reduced the fossil fuel consumption and thereby the NO_x
676 emissions from the power sector. During industrial shutdowns and production
677 restrictions caused by the epidemic, frequent start-ups and shutdowns of production
678 and pollution control equipment resulted in a clear decline in NO_x removal efficiency

679 compared with normal operation condition of selective catalytic reduction (SCR)
680 systems. Previous measurements found that the average NO_x removal efficiency of
681 coal-fired units in iron & steel production enterprises decreased from 78% to 61%
682 (Shao et al., 2023), which to some extent offset the emission reduction effect of
683 industrial sources due to production restrictions.

684 SO₂ emission reductions predominantly originated from power (521 Mg, 21%) and
685 industrial sectors (1,710 Mg, 68%). For PM_{2.5}, transportation contributed 56% to the
686 total reduction of 3,583 Mg, with the contributions from on-road transportation,
687 construction machinery, marine, railway, and aviation accounting for 8%, 18%, 14%,
688 9%, and 7%, respectively. The emission reductions of NMVOCs were estimated at
689 20,170 Mg. The contribution of industrial sources reached 93%, largely due to a 64%
690 decline in crude oil processing in Jiangsu Province compared to 2023, as well as the
691 substantial declines in the production of chemical products (e.g., 27% less in
692 chemicals fibers and 65% less in ethylene manufacturing, NBS, 2023). The results
693 emphasized the lockdown impact on petrochemical industries reliant on cross-regional
694 material flows. In contrast, the emissions from residential sector were larger for the
695 lockdown period, with its coal consumption 7% more than that in recovery period one
696 year later, likely driven by the enhanced heating/cooking demands during mobility
697 restrictions.

698 In addition, an examination was conducted for exploring the diverse rebounds of
699 emissions for different sectors. Vehicle emissions exhibited a clear growth in May
700 compared to the central lockdown period in April. This early rebound in transportation
701 was likely driven by the gradual recovery of essential logistics and commuting. In
702 contrast, the emissions from industrial sector remained at a greatly suppressed level
703 throughout April and May, without an immediate rebound. This lag in industrial
704 recovery aligned with the socioeconomic condition of YRD, where the regional
705 industrial added value and GDP experienced a substantial decline in the second
706 quarter of 2022, followed by a slow recovery in the subsequent months (JSBS, 2022).
707 Such diversity between sectors indicated that mobile sources and energy supply could

708 respond quickly to the lifting of restrictions, while the recovery of large-scale
709 manufacturing could be more difficult due to complex supply chain realignment.

710 To further explore the spatial heterogeneity of the lockdown impacts, we conducted a
711 city-level comparative analysis by selecting three representative cities: Suzhou in
712 southern Jiangsu, Nantong in central Jiangsu, and Xuzhou in northern Jiangsu (see
713 locations of the cities in Figure S1). Suzhou is adjacent to Shanghai, with dense
714 petrochemical and manufacturing industries deeply embedded in regional supply
715 chains. Nantong is located in coastal area and relies heavily on marine logistics and
716 ports. Xuzhou is a city dominated by heavy industries and is farther from Shanghai
717 with less direct lockdown exposure compared to other cities in Jiangsu.

718 As a core economic hub deeply integrated with Shanghai's supply chain, Suzhou was
719 greatly influenced by Shanghai lockdown (Table S2). The NMVOCs and NO_x
720 emissions in April-May 2022 dropped 17.9% (6,812 Mg) and 15.2% (2,917 Mg),
721 respectively, compared to the normal level (April-May 2023). This acute decline was
722 co-driven by the near-total freeze of cross-city highway freight, massive operational
723 bottlenecks at major ports, and widespread suspensions of petrochemical and
724 electronics manufacturing. Meanwhile, there existed notable drops in PM_{2.5} (-13.0%)
725 and SO₂ emissions (-9.0%) from halted construction and industrial fuel use. In
726 Nantong, the moderate declines in NO_x (-9.2%), NMVOCs (-8.6%), PM_{2.5} (-6.8%)
727 and SO₂ (-4.9%) primarily reflected disruptions in regional waterway logistics and
728 slowdowns in general manufacturing. In contrast, the emission reductions in Xuzhou
729 were much smaller around 3%, attributed to the continuous operations of heavy
730 industry to maintain the essential supply chains of industrial economy. These
731 diversities between cities demonstrated the capability of the research framework to
732 track the emission variation due to temporal and/or unexpected events at relatively
733 high spatiotemporal resolution.

734 In a summary, the results revealed complicated and diverse interventions of public
735 health incidents on energy use and activities for different sectors. The near-real-time
736 techniques developed in this work proved capable to capture the fast response of air

737 pollutant emissions to the short-term measures conducted during unexpected incidents,
738 and to clear identify the driving sectors of emission changes compared to the normal
739 conditions.

740 **3.3 Evaluation of the near-real-time emission estimates with air** 741 **quality simulation**

742 The near-real-time estimates of provincial emissions were evaluated with air quality
743 simulation with CMAQ. To assess model performance, the observed concentrations of
744 hourly SO₂, NO₂, PM_{2.5}, and MDA8 O₃ were compared with the simulations based on
745 the provincial-level near-real-time emission estimates and MEIC for the selected four
746 months of 2022, as summarized in Supplementary Table S3. Overall, the simulation
747 with the provincial emission estimates shows acceptable agreement with the
748 observations, with the annual means of NMB and NME ranging -37.1% – 24.1% and
749 33.7% –53.5% for SO₂, -20.2% – 27.0% and 15.9% – 36.2% for NO₂, -18.6% – 10.8%
750 and 37.5% –62.5% for PM_{2.5}, and -41.2% – -23.1% and 32.7% – 49.3% for O₃. The
751 analogous numbers for MEIC were -33.4% – 25.5% and 40.9% –51.8% for SO₂, -19.9%
752 – 35.6% and 22.3% – 55.1% for NO₂, -8.6% – 25.2% and 37.5% – 52.5% for PM_{2.5},
753 and -39.9% – -28.1% and 44.3% – 54.5% for O₃, respectively. Most of the NMB and
754 NME were within the recommended criteria ($-30\% \leq \text{NMB} \leq 30\%$ and $\text{NME} \leq 50\%$,
755 Emery et al., 2017). Better performance was achieved using the provincial emission
756 estimates developed in this work, implying the benefit of applying the refined
757 emission data on high-resolution air quality simulation.

758 Figures 6 and 7 compares the simulated daily PM_{2.5} and O₃ concentrations based on
759 the provincial (this work) and national emission estimates (MEIC) against
760 observations (results for SO₂ and NO₂ are shown in Supplementary Figures S5 and S6,
761 while spatial distributions for all the four pollutants are provided in Supplementary
762 Figures S7-S10). Compared to MEIC, the provincial-scale emission estimates
763 demonstrated better model performance in capturing the daily variability of pollutant
764 concentrations. The greater correlation coefficients (R) between simulated and

765 observed concentrations based on the near-real-time estimates indicated a remarkable
766 improvement for all the involved air pollutants (Table S3).

767 Figure 6 compares the observed and simulated PM_{2.5} concentrations, and measurable
768 improvement of model performance was achieved with the updated temporal profiles
769 for emissions. Specifically, the NMEs for January, April, July, and October decreased
770 from 37.5%, 55.3%, 62.5%, and 51.3% to 33.2%, 29.2%, 48.1%, and 42.6%,
771 respectively. The greatly improved model performance for April 2022 demonstrated
772 the capability of the near-real-time emission data to better capture the influence of
773 temporarily disrupted anthropogenic activities on air quality. During this period, the
774 COVID-19 lockdown in Shanghai severely restricted cross-regional freight transport
775 and industrial operations in Jiangsu (Huang et al., 2021). Compared with previous
776 emission inventories relying on historical temporal patterns, the refined daily emission
777 inventory with near-real-time techniques provided a more realistic representation of
778 the decline in primary aerosols and precursor emissions from heavy-duty vehicles and
779 point sources. Consequently, the simulated PM_{2.5} concentrations showed better
780 agreement with observations, with the NMB reduced to -6.6%. The refined emission
781 inventory also yielded notable corrections for periods with targeted administrative
782 interventions. During the late July period (July 20 to 31), for example, the NMB for
783 PM_{2.5} decreased from 47.3% with MEIC to 16.1% with the near-real-time emission
784 data, and the simulated mean concentrations dropped from 76.4 to 60.2 $\mu\text{g}/\text{m}^3$, much
785 closer to the observed 52.0 $\mu\text{g}/\text{m}^3$. This improvement was likely attributable to the
786 inventory's dynamic response to official electricity rationing policy. Driven by
787 extreme summer heat waves and power grid stress, local governments mandated load
788 reduction measures for energy-intensive facilities (Wei et al., 2020), causing an
789 irregular drop in industrial emissions that may not be tracked in previous inventories.
790 Similarly, the clear overestimation with MEIC for October was effectively mitigated.
791 The refined emission data appeared to better reflect the benefit of stringent control
792 measures implemented for preventing the heavy haze pollution in autumn and winter
793 (Jiang et al., 2023).

794 Figure 7 presents the observed and simulated O₃ concentrations. Compared with
795 MEIC, the NMEs with the near-real-time emission data for January, April, July, and
796 October decreased from 51.4%, 54.0%, 44.3%, and 54.5% to 49.3%, 41.1%, 32.7%,
797 and 34.6%, respectively. The updated emission data could have modulated the
798 simulation of non-linear photochemical processes. In January when weak solar
799 radiation generally limits photochemical O₃ production, NO_x titration often acts as a
800 dominating mechanism. The simulation with MEIC underestimated NO₂ by 37.4%,
801 and it potentially contributed to a 36.0% overestimation of O₃ due to insufficient
802 chemical scavenging. With the NO_x emissions 12% higher than MEIC during the
803 January, the near-real-time emission inventory resulted in a more reasonable
804 simulation of the titration effect. The enhanced chemical sink reduced the O₃ NMB to
805 -23.1% and improved the R² from 0.30 to 0.66. For April, the NO_x emissions were
806 15.9% lower in the real-near-time inventory than MEIC. Such a reduction in NO_x
807 could effectively weaken the titration inhibition, and it likely allowed the model to
808 better track the accelerated accumulation of O₃ driven by increasing spring solar
809 radiation. Simulation with the refined emission data yielded a growth of 1.72 μg/m³
810 for the month, much closer to the observation (2.59 μg/m³) than that with MEIC (0.33
811 μg/m³). Furthermore, there existed substantial correction of O₃ underestimation in
812 October, with the NME reduced from 54.5% to 34.6%. Such improvement resulted
813 potentially from the better simulated aerosol-radiation feedback. As mentioned earlier,
814 specific measures were conducted during autumn and winter in Jiangsu to prevent
815 heavy haze pollution. The emission abatement resulting from those measures were
816 captured by the near-real-time techniques, facilitating a lower aerosol loading in
817 CMAQ simulation compared to that with MEIC. This could theoretically elevate
818 photochemistry process and accelerate O₃ production, partially bridging the gap
819 between simulation and observation. In contrast, MEIC did not fully include the local
820 pollution control measures for specific seasons, and the relatively high aerosol loading
821 from simulation might have overly suppressed photochemical O₃ formation by
822 scattering and absorbing actinic flux (Zhao et al., 2021).

823 **3.4 Impact of daily emission change on the variability of PM_{2.5} and O₃**
824 **concentrations**

825 **3.4.1 Anthropogenic-driven contributions to variability of PM_{2.5} and MDA8 O₃**
826 **concentrations**

827 Figure 8 presents the contributions of the changing daily emissions to the monthly
828 variability of PM_{2.5} and MDA8 O₃ concentrations based on the MLR model. The
829 model performance was assessed with observed PM_{2.5} and O₃ concentrations
830 (Supplementary Figure S11). The simulated concentrations were strongly correlated
831 with observational data, with the correlation coefficient (R) of 0.79 for PM_{2.5} and 0.88
832 for MDA8 O₃. The validation indicated satisfying performance of MLR in capturing
833 provincial air quality variability.

834 The anthropogenic-driven variability of PM_{2.5} concentration was basically consistent
835 with the temporal variation of estimated emissions. As shown in Figure 8a, the
836 abundant emissions in January resulted in a prominent enhancement of 12.7 µg/m³ for
837 PM_{2.5} concentration, followed by December (1.8 µg/m³) and June (1.6 µg/m³). In
838 particular, the enhancement of June was driven largely by the post-pandemic
839 economic recovery, as discussed in in Section 3.2. For most warm months (April to
840 October, except June), negative impacts of anthropogenic activities on PM_{2.5} level
841 were found, ranging 1.1 – 4.2 µg/m³. Clear decline of PM_{2.5} due to emission change
842 was also found in February (5.5 µg/m³), resulting probably from the greatly reduced
843 human activities (industry and transportation) during the Chinese New Year holiday.
844 The PM_{2.5} growth occurred during winter heating period highlighted the necessity of
845 accelerating transition of clean household energy and improving management of
846 industrial production after the short-term lockdowns.

847 The variation of anthropogenic emissions was found to elevate O₃ concentrations in
848 most months of the year, particularly for warm seasons (Figure 8b). The
849 enhancements during March-August ranged 0.8 – 3.8 µg/m³, suggesting the important
850 role of human activities in aggravating O₃ pollution. High temperature in summer

851 promoted the emissions of temperature-dependent O₃ precursors, particularly
852 NMVOCs from various sources (Figure 2d). In addition, the NO_x emissions from
853 certain sources were elevated in warm seasons, e.g., those from off-road machinery in
854 the summer harvest season (Figure 2a). The growing abundance of precursors,
855 together with high temperature, enhanced the photochemical production rate of O₃.

856 However, the anthropogenic emissions during winter demonstrated a net negative
857 contribution to surface O₃ concentrations (e.g., -6.2 and -2.4 µg/m³ for November and
858 December, respectively), indicating a shift in the chemical regime of O₃ formation.
859 Although the NO_x emissions were not enhanced in winter (Figure 4), the weak
860 photochemical production under low temperature and solar radiation made the NO_x
861 titration more dominating in O₃ chemistry, primarily resulting in this net negative
862 contribution. Simultaneously, reduced NMVOCs emissions and diminished
863 photochemical activity restricted the efficiency of radical-driven O₃ production. The
864 resulting O₃-depleting reactions overwhelmed potential formation mechanisms,
865 leading to the estimated negative contribution from anthropogenic emissions. This
866 pattern contrasted sharply with the net positive effect of anthropogenic activities in
867 summer months, and underscored the complex season-dependent response of O₃ level
868 to the changing precursor emissions.

869 **3.4.2 Impact of fluctuations in anthropogenic emissions by precursor and sector** 870 **on PM_{2.5} and MDA8 O₃ concentrations**

871 The impacts of anthropogenic emission fluctuations on variability of PM_{2.5} and O₃
872 concentrations were quantified by precursor and sector, with a machine learning
873 framework integrating XGBoost and SHAP analysis. Derived from the 10-fold cross
874 validation, the correlation coefficient (R) between machine learning prediction and
875 observation reached 0.78 and 0.81 for daily PM_{2.5} and MDA8 O₃, respectively,
876 suggested satisfying capability of the machine learning framework in predicting the
877 anthropogenic-driven variability of PM_{2.5} and O₃ concentrations (Supplementary
878 Figure S12).

879 Figure 9a and 9b illustrates the contributions of changing emissions from different
880 pollutant-sector combinations to the variability of PM_{2.5} concentration in January and
881 that of MDA8 O₃ in July, respectively. The temporal variability of PM_{2.5} level
882 attributable to anthropogenic emission changes was in general consistent with that of
883 observed surface PM_{2.5} concentration (Figure 9a). For O₃, there existed some
884 discrepancy between the temporal distribution of anthropogenic-driven variability and
885 observed concentration in summer. This discrepancy may be attributed to the
886 substantial impacts of meteorological conditions and biogenic VOCs emissions on O₃
887 formation (Gu et al., 2023).

888 Among all the pollutant-sector combinations, fluctuations in agricultural NH₃
889 emissions accounted for 67.3% of the variability of PM_{2.5} concentrations in January,
890 followed by off-road NO_x (12.9%) and residential PM_{2.5} emissions (4.9%). The
891 contribution of NH₃ emission variation significantly exceeded those of NO_x (17.7%),
892 PM_{2.5} (10.8%), and SO₂ (4.2%), suggesting that Jiangsu may be transitioning to an
893 NH₃-rich regime following substantial reductions in SO₂ and NO_x emissions (Zhao et
894 al., 2020b). Therefore, agricultural NH₃ control has become the priority of the strategy
895 design for PM_{2.5} pollution alleviations, compared to traditional NO_x abatement. The
896 fluctuations in VOC-Industry contributed to 48.5% of the variability of MDA8 O₃
897 concentrations in July, followed by off-road VOCs (9.7%) and NO_x emissions (8.9%).
898 In total, the NMVOCs accounted for 69.7% of the anthropogenic-driven variability of
899 O₃ concentration, exceeding the contributions from NO_x (14.5%), PM_{2.5} (11.0%), and
900 SO₂ (4.9%). The positive contribution of NO_x to MDA8 O₃ indicated that the O₃
901 formation mechanism in Jiangsu may be shifting from a VOCs-limited regime
902 towards a transitional or NO_x-limited regime. Regarding the sector contributions with
903 various species aggregated, the agricultural emission fluctuations contributed most to
904 anthropogenic-driven variability of PM_{2.5} concentration (67.3%, Figure 9c), while
905 industrial activities contributed most to that of O₃ concentration (54.8%, Figure 9d).
906 Notably, off-road transportation emerged as an important contributor to both
907 pollutants (15.6% for PM_{2.5} and 24.4% for O₃), providing clear evidence for policy
908 making of coordinating control of PM_{2.5} and O₃ pollution.

909 4. Concluding remarks

910 In this study, we incorporated near-real-time activity data from multiple sources and
911 developed a method framework for continuously estimating the regional daily air
912 pollutant emissions of anthropogenic origin. We then applied this method to estimated
913 the spatiotemporal evolution of emissions in Jiangsu Province, a typical developed
914 area in eastern China, with a particular focus on the period during the COVID-19
915 lockdown in 2022 and the corresponding phase-period after the lifting of restrictions
916 in 2023. Finally, we constructed a rapid assessment approach that utilized machine
917 learning algorithms to quantify the impact of fast changing emissions on variability of
918 daily air quality ambient concentrations of PM_{2.5} and O₃.

919 Our research We indicated that emission controls have played a crucial role in
920 abatement of air pollutant emissions. The provincial emissions of SO₂, NO_x, PM_{2.5},
921 NMVOCs, and NH₃ decreased 17%, 33%, 18%, 7%, and 11%, respectively, from
922 2019 to 2022. Implementation of ultra-low emission retrofits for industrial sectors has
923 proven effective in reducing primary PM_{2.5} and NO_x emissions. However, there is an
924 urgent need to enhance NMVOCs emission control in key industrial sectors and areas.

925 We identified distinct Regarding the temporal variabilities of emissions for various air
926 pollutants, The emissions of SO₂ and PM_{2.5} were influenced greatly by fossil fuel

927 consumption pattern, while NO_x emissions were increasingly dominated by that of
928 transportation. The NMVOCs emissions peaked in the summer and declined in winter,

929 followed by a rebound in emissions after the Chinese New Year. Our eComparative
930 analysis indicated showed that the emissions of NO_x, SO₂, PM_{2.5}, and NMVOCs in

931 Jiangsu during the COVID-19 lockdown of Shanghai in April-May 2022 were
932 respectively 8%, 6%, 6%, and 10% smaller than those in the same months of 2023.

933 Transportation was identified as the primary contributors to the reductions in NO_x and
934 PM_{2.5} emissions, while industry accounted for 93% of the reduction in NMVOCs,

935 closely associated with the disrupted cross-regional product supply chains. Indicated
936 by the contributions of changing emissions from pollutant-sector combinations to the

937 variability of PM_{2.5} and O₃ levels concentrations, reducing agricultural NH₃ emissions

938 should be critical for PM_{2.5} pollution alleviation, and off-road transportation has
939 become a priority target for coordinating control of both PM_{2.5} and O₃ pollution.
940 The near-real-time techniques and estimation of daily-level emissions offer substantial
941 practical implications for current air quality management in China. Specifically, it can
942 be directly integrated into the “Emergency Response for Reducing Heavy Pollution
943 Weather” program. By providing the near-real-time feedback on emission variations,
944 policy makers can reasonably determine the short-term emission reduction measures
945 and timely evaluate their actual effectiveness (e.g., temporary suspension of specific
946 ~~industries~~ industrial or traffic restrictions). Furthermore, combined with machine
947 learning techniques, this framework allows policy makers to decouple ~~and distinguish~~
948 the environmental benefits of long-term policies of air quality improvement from
949 short-term emergency controls or unexpected socioeconomic shocks (like the
950 COVID-19 lockdown). The obtained knowledge provides a scientific basis for
951 formulating more cost-effective and ~~precise-reasonable~~ coordinated control-strategies
952 for coordinating the reducing-PM_{2.5} and O₃ pollution controls.
953 Furthermore, the framework could be potentially applied for predicting future
954 ~~emission~~ emission under various hypothetical scenarios. ~~Because~~ as the framework ~~it~~
955 establishes a dynamic linkage between sector-specific activity factors and emissions,
956 ~~it could theoretically serve as a tool for predicting the emission change from policy~~
957 ~~formulation~~. By adjusting these activity factors, (such as the ~~gradual~~ penetration of
958 electric ~~heavy-duty~~ vehicles, the ~~abatement of implementation of various~~ industrial
959 production ~~abatement~~ during haze events, ~~or~~ and targeted reductions in agricultural
960 activities), researchers and policy-makers could fast and reasonably project the
961 ~~emission-levels~~ of diverse future scenarios. Coupled with the rapid assessment
962 approach with machine learning, the framework presents a promising pathway to
963 quantify how the ~~simulated~~ emission changes might affect the daily variability of air
964 quality, thereby better supporting the policy design and adjustment for regional
965 complex pollution controls.
966 The limitations of this work existed mainly in the near-real-time information of
967 multiple sources and the rapid assessment of air quality variability. For instance,

968 CEMS ~~were only applied covered only for relatively~~ big point sources, thus we had to
969 assume that the small and fugitive sources followed similar variability of emissions
970 ~~with as~~ point sources. As CEMS only covers SO₂, ~~PM_{2.5}, and~~ NO_x, ~~and particles~~, the
971 use of electricity consumption data for NMVOCs may introduce substantial
972 uncertainty. Future improvement in online monitoring of NMVOCs will enhance the
973 estimation of temporal variation of emissions. While our research framework
974 demonstrates robust performance in ~~data-rich regions like~~ Jiangsu Province, its heavy
975 reliance on ~~extensive~~ CEMS ~~coverage~~ and provincial traffic monitors poses a
976 limitation for its transferability to less developed regions or other developing
977 countries without sufficient data support. To adapt this methodology for those regions,
978 future applications could be expanded to other datasets with global accessibility. For
979 instance, satellite-derived tropospheric NO₂ columns, daily nighttime light
980 fluctuations, and generalized mobile phone signaling data could serve as alternative
981 proxies to estimate the activity levels and their temporal profiles. Expanding this
982 framework to incorporate such multi-source remote sensing data will be more crucial
983 for establishing near-real-time emission inventories in regions with less data support.
984 Moreover, the machine learning process ignored the contributions from regional
985 transport, which could result in some bias in analyzing the impacts of anthropogenic
986 emissions on air quality. However, in contrast to time-consuming numerical modeling,
987 machine learning offered a rapid and reliable assessment of the impact of daily
988 emission changes on air quality, ~~which exactly addressed the requirement of air~~
989 ~~quality management~~, and was thus recommended in future policy making of air
990 pollution controls.

991 **Data availability**

992 The gridded emission data for Jiangsu Province 2022-2023 can be downloaded at
993 <http://www.airqualitynju.com>

994 **Author contributions**

995 CGu developed the methodology, conducted the research and wrote the draft. YZhao
996 and LZhang developed the strategy and designed the research, and YZhao revised the
997 manuscript. YWang provided the support of machine learning modeling. YJi provided
998 the support of WFR-CMAQ. ZZhang, and WZhao supported emission data processing.
999 SSun, YBian, JZhu, and SZhong provided the support of emission data.

1000 **Competing interests**

1001 The authors declare that they have no conflict of interest.

1002 **Acknowledgments**

1003 This work was sponsored by the National Natural Science Foundation of China (grant
1004 no. 42577116), the National Key Research and Development Program of China
1005 (2023YFC3709802), the Key Research and Development Programme of Jiangsu
1006 Province (BE2022838), and the Key Laboratory of Formation and Prevention of
1007 Urban Air Pollution Complex, Ministry of Ecology and Environment (no.
1008 2025080167).

1009 **References**

1010 An, J., Huang, Y., Huang, C., Wang, X., Yan, R., Wang, Q., Wang, H., Jing, S., Zhang,
1011 Y., Liu, Y., Chen, Y., Xu, C., Qiao, L., Zhou, M., Zhu, S., Hu, Q., Lu, J., and
1012 Chen, C.: Emission inventory of air pollutants and chemical speciation for
1013 specific anthropogenic sources based on local measurements in the Yangtze
1014 River Delta region, China, *Atmos. Chem. Phys.*, 21, 2003–2025,
1015 <https://doi.org/10.5194/acp-21-2003-2021>, 2021.

1016 BEIS: Provisional UK greenhouse gas emissions national statistics,
1017 <https://www.gov.uk/government/statistics/> (last visited on October 2025), 2022.

1018 Bo, X., Jia, M., Xue, X., Tang, L., Mi, Z., Wang, S., Cui, W., Chang, X., Ruan, J.,

1019 Dong, G., Zhou, B., and Davis, S.: Effect of strengthened standards on Chinese
1020 ironmaking and steelmaking emissions, *Nat. Sustain.*, 4, 811-820,
1021 <https://doi.org/10.1038/s41893-021-00736-0>, 2021.

1022 Carbon monitor: Global high spatial resolution near real time carbon map,
1023 <https://www.carbonmonitor.org.cn/> (last visited on October 2025), 2024.

1024 CBS: Emissions of greenhouse gases according to IPCC guidelines, quarter,
1025 <https://www.cbs.nl/nl-nl/cijfers/detail/> (last visited on October 2025), 2024.

1026 Chu, B., Ma, Q., Liu, J., Ma, J., Zhang, P., Chen, T., Feng, Q., Wang, C., Yang, N., Ma,
1027 H., Ma, J., Russell, A. G., and He, H.: Air Pollutant Correlations in China:
1028 Secondary Air Pollutant Responses to NO_x and SO₂ Control, *Environ. Sci.*
1029 *Technol. Lett.*, 7, 695-700, <https://doi.org/10.1021/acs.estlett.0c00403>, 2020.

1030 CITEPA: Monthly emissions barometer, <https://www.citepa.org/fr/barometre/> (last
1031 access: October 2025), 2024.

1032 Cliff, S. J., Drysdale, W., Lee, J. D., Helfter, C., Nemitz, E., Metzger, S., and Barlow,
1033 J. F.: Pandemic restrictions in 2020 highlight the significance of non-road NO_x
1034 sources in central London, *Atmos. Chem. Phys.*, 23, 2315–2330,
1035 <https://doi.org/10.5194/acp-23-2315-2023>, 2023.

1036 Crippa, M., Solazzo, E., Huang G., Guizzardi D., Koffi E., Muntean M., Schieberle C.,
1037 Friedrich R.: High resolution temporal profiles in the Emissions Database for
1038 Global Atmospheric Research, *Sci. Data*, 7, 121,
1039 <https://doi.org/10.1038/s41597-020-0462-2>, 2020.

1040 Department of Ecology and Environment of Jiangsu province (DEE).: Report on the
1041 State of the Ecology and Environment in Jiangsu province, 2023.

1042 Department of Ecology and Environment of Jiangsu province (DEE).: Emergency
1043 Plan for Severe Air Pollution in Jiangsu Province, 2022.

1044 Department of Industry and Information Technology of Jiangsu province (DII).:
1045 Notice on Enterprises and Vehicles Intending to Apply for the 2022 Central
1046 Government Subsidy Settlement Fund for the Promotion and Application of New
1047 Energy Vehicles, 2023.

1048 Ding, J., van der A, R. J., Mijling, B., Levelt, P. F., and Hao, N.: NO_x emission

1049 estimates during the 2014 Youth Olympic Games in Nanjing, *Atmos. Chem.*
1050 *Phys.*, 15, 9399–9412, <https://doi.org/10.5194/acp-15-9399-2015>, 2015.

1051 Dong, X., Zhang, Y., Yu, G., Xiong, Y., Han, Z., Huo, J., Huang, C., Kan, H., Zheng,
1052 M., Ning, Z., and Xie, B.: Environmental and health impacts of reduced PM_{2.5}
1053 and trace metals from ship emissions under low-sulfur fuel oil policy in Shanghai,
1054 China, *Environmental Pollution*, 377, 126409,
1055 <https://doi.org/10.1016/j.envpol.2025.126409>, 2025.

1056 Dou, X., Wang, Y., Ciais, P., Chevallier, F., Davis, S. J., Crippa, M.,
1057 Janssens-Maenhout, G., Guizzardi, D., Solazzo, E., Yan, F., Huo, D., Zheng, B.,
1058 Zhu, B., Cui, D., Ke, P., Sun, T., Wang, H., Zhang, Q., Gentine, P., Deng, Z., and
1059 Liu, Z.: Near-real-time global gridded daily CO₂ emissions, *The Innovation*, 3,
1060 100182, <https://doi.org/10.1016/j.xinn.2021.100182>, 2022.

1061 Emery, C., Liu, Z., Russell, A. G., Odman, M. T., Yarwood, G., and Kumar, N.:
1062 Recommendations on statistics and benchmarks to assess photochemical model
1063 performance, *J. Air Waste Manag. Assoc.*, 67, 582-598,
1064 <https://doi.org/10.1080/10962247.2016.1265027>, 2017.

1065 Gaubert, B., Bouarar, I., Doumbia, T., Liu, Y., Stavrakou, T., Deroubaix, A., Darras, S.,
1066 Elguindi, N., Granier, C., Lacey, F., Müller, J. F., Shi, X., Tilmes, S., Wang, T.,
1067 and Brasseur, G. P.: Global changes in secondary atmospheric pollutants during
1068 the 2020 COVID-19 pandemic, *J. Geophys. Res. Atmos.*, 126, e2020JD034213.
1069 <https://doi.org/10.1029/2020JD034213>, 2021.

1070 Geng, G., Xiao, Q., Liu, S., Liu, X., Cheng, J., Zheng, Y., Xue, T., Tong, D., Zheng, B.,
1071 Peng, Y., Huang, X., He, K., and Zhang, Q.: Tracking Air Pollution in China:
1072 Near Real-Time PM_{2.5} Retrievals from Multisource Data Fusion, *Environ. Sci.*
1073 *Technol.*, 55, 12106-12115, <https://doi.org/10.48550/arXiv.2103.06520>, 2021.

1074 Geng, G., Liu, Y., Liu, Y., Liu, S., Cheng, J., Yan, L., Wu, N., Hu, H., Tong, D., Zheng,
1075 B., Yin, Z., He, K., and Zhang, Q.: Efficacy of China's clean air actions to tackle
1076 PM_{2.5} pollution between 2013 and 2020, *Nature Geoscience*, 17, 987–994,
1077 <https://doi.org/10.1038/s41561-024-01540-z>, 2024.

1078 Gu, C., Zhang, L., Xu, Z., Xia, S., Wang, Y., Li, L., Wang, Z., Zhao, Q., Wang, H., and

1079 Zhao, Y.: High-resolution regional emission inventory contributes to the
1080 evaluation of policy effectiveness: a case study in Jiangsu Province, China,
1081 *Atmos. Chem. Phys.*, 23, 4247–4269, <https://doi.org/10.5194/acp-23-4247-2023>,
1082 2023.

1083 Guevara, M., Jorba, O., Soret, A., Petetin, H., Bowdalo, D., Serradell, K., Tena, C.,
1084 Denier van der Gon, H., Kuenen, J., Peuch, V.-H., and Pérez García-Pando, C.:
1085 Time-resolved emission reductions for atmospheric chemistry modelling in
1086 Europe during the COVID-19 lockdowns, *Atmos. Chem. Phys.*, 21, 773–797,
1087 <https://doi.org/10.5194/acp-21-773-2021>, 2021.

1088 Guevara, M., Petetin, H., Jorba, O., Denier van der Gon, H., Kuenen, J., Super, I.,
1089 Granier, C., Doumbia, T., Ciais, P., Liu, Z., Lamboll, R. D., Schindlbacher, S.,
1090 Matthews, B., and Pérez García-Pando, C.: Towards near-real-time air pollutant
1091 and greenhouse gas emissions: lessons learned from multiple estimates during
1092 the COVID-19 pandemic, *Atmos. Chem. Phys.*, 23, 8081–8101,
1093 <https://doi.org/10.5194/acp-23-8081-2023>, 2023.

1094 Harkins, C., McDonald, B. C., Henze, D. K., and Wiedinmyer, C.: A fuel-based
1095 method for updating mobile source emissions during the COVID-19 pandemic,
1096 *Environ. Res. Lett.*, 16, 065018, <https://doi.org/10.1088/1748-9326/ac0660>,
1097 2021.

1098 He K., Zhang Q., Wang S.: Technical manual for the preparation of urban air pollution
1099 Source emission inventory, China Statistics Press, Beijing, 2018 (in Chinese).

1100 Hu, W., Zhao, Y., Lu, N., Wang, X., Zheng, B., Henze, D. K., Zhang, L., Fu, T.-M.,
1101 and Zhai, S.: Changing Responses of PM_{2.5} and Ozone to Source Emissions in
1102 the Yangtze River Delta Using the Adjoint Model, *Environ. Sci. Technol.*, 58,
1103 628-638, <https://doi.org/10.1021/acs.est.3c05049>, 2024.

1104 Huang, C., An, J., Wang, H., Liu, Q., Tian, J., Wang, Q., Hu, Q., Yan, R., Shen, Y.,
1105 Duan, Y., Fu, Q., Shen, J., Ye, H., Wang, M., Wei, C., Cheng, Y., and Su, H.:
1106 Highly Resolved Dynamic Emissions of Air Pollutants and Greenhouse Gas CO₂
1107 during COVID-19 Pandemic in East China, *Environ.Sci.Technol.Lett.*, 8,
1108 853-860, <https://doi.org/10.1021/acs.estlett.1c00600>, 2021.

1109 Huo, D., Huang, X., Dou, X., Ciais, P., Li, Y., Deng, Z., Wang, Y., Cui, D., Benkhelifa,
1110 F., Sun, T., Zhu, B., Roest, G., Gurney, K. R., Ke, P., Guo, R., Lu, C., Lin, X.,
1111 Lovell, A., Appleby, K., DeCola, P. L., Davis, S. J., and Liu, Z.: Carbon Monitor
1112 Cities near-real-time daily estimates of CO₂ emissions from 1500 cities
1113 worldwide, *Sci. Data*, 9, 533, <https://doi.org/10.1038/s41597-022-01657-z>, 2022.

1114 Jiang, S., Kong, S., Zheng, H., Wu, J., Yao, L., Chen, N., Zhu, B., Zhao, T., Bai, Y.,
1115 Liu, D., and Qi, S.: Winter-autumn air pollution control plan in North China
1116 modified the PM_{2.5} compositions and sources in Central China, *Atmos. Environ.*,
1117 306, 119827, <https://doi.org/10.1016/j.atmosenv.2023.119827>, 2023.

1118 Kholod, N., Evans, M., Gusev, E., Yu, S., Malyshev, V., and Barinov, A.: A
1119 methodology for calculating transport emissions in cities with limited traffic data:
1120 Case study of diesel particulates and black carbon emissions in Murmansk, *Sci.*
1121 *Total Environ.*, 547, 305-313, <https://doi.org/10.1016/j.scitotenv.2015.12.151>,
1122 2016.

1123 Kurokawa, J. and Ohara, T.: Long-term historical trends in air pollutant emissions in
1124 Asia: Regional Emission inventory in ASia (REAS) version 3, *Atmos. Chem.*
1125 *Phys.*, 20, 12761–12793, <https://doi.org/10.5194/acp-20-12761-2020>, 2020.

1126 Lei, T., Wang, D., Yu, X., Ma, S., Zhao, W., Cui, C., Meng, J., Tao, S., and Guan, D.:
1127 Global iron and steel plant CO₂ emissions and carbon-neutrality pathways,
1128 *Nature*, 622, 514–520, <https://doi.org/10.1038/s41586-023-06486-7>, 2023.

1129 Li, K., Jacob, D. J., Shen, L., Lu, X., De Smedt, I., and Liao, H.: Increases in surface
1130 ozone pollution in China from 2013 to 2019: anthropogenic and meteorological
1131 influences, *Atmos. Chem. Phys.*, 20, 11423–11433,
1132 <https://doi.org/10.5194/acp-20-11423-2020>, 2020.

1133 Li, K., Jacob, D. J., Liao, H., Qiu, Y., Shen, L., Zhai, S., Bates, K. H., Sulprizio, M. P.,
1134 Song, S., Lu, X., Zhang, Q., Zheng, B., Zhang, Y., Zhang, J., Lee, H. C., and Kuk,
1135 S. K.: Ozone pollution in the North China Plain spreading into the late-winter
1136 haze season, *Proc. Natl. Acad. Sci.*, 118, e2015797118,
1137 <https://doi.org/10.1073/pnas.2015797118>, 2021.

1138 Li, M., Zhang, Q., Zheng, B., Tong, D., Lei, Y., Liu, F., Hong, C., Kang, S., Yan, L.,

1139 Zhang, Y., Bo, Y., Su, H., Cheng, Y., and He, K.: Persistent growth of
1140 anthropogenic non-methane volatile organic compound (NMVOC) emissions in
1141 China during 1990–2017: drivers, speciation and ozone formation potential,
1142 *Atmos. Chem. Phys.*, 19, 8897–8913, <https://doi.org/10.5194/acp-19-8897-2019>,
1143 2019.

1144 Li, H. and Zheng, B.: TROPOMI NO₂ Shows a Fast Recovery of China’s Economy in
1145 the First Quarter of 2023, *Environ. Sci. Technol. Lett.*, 10, 635-641,
1146 <https://doi.org/10.1021/acs.estlett.3c00386>, 2023.

1147 Liu, F., Page, A., Strode, S. A., Yoshida, Y., Choi, S., Zheng, B., Lamsal, L. N., Li, C.,
1148 Krotkov, N. A., Eskes, H., van der A, R., Veefkind, P., Levelt, P. F., Hauser, O. P.,
1149 and Joiner, J.: Abrupt decline in tropospheric nitrogen dioxide over China after
1150 the outbreak of COVID-19, *Sci. Adv.*, 6, eabc2992,
1151 <https://doi.org/10.1126/sciadv.abc2992>, 2020.

1152 Liu, M., Shang, F., Lu, X., Huang, X., Song, Y., Liu, B., Zhang, Q., Liu, X., Cao, J.,
1153 Xu, T., Wang, T., Xu, Z., Xu, W., Liao, W., Kang, L., Cai, X., Zhang, H., Dai, Y.,
1154 and Zhu, T.: Unexpected response of nitrogen deposition to nitrogen oxide
1155 controls and implications for land carbon sink, *Nat. Commun.*, 13, 3126,
1156 <https://doi.org/10.1038/s41467-022-30854-y>, 2022.

1157 Liu, X., Yang, L., Du, J., Zhang, H., Hu, J., Chen, A., and Lv, W.: Carbon and air
1158 pollutant emissions forecast of China's cement industry from 2021 to 2035,
1159 *Resources, Conservation and Recycling*, 204, 107498,
1160 <https://doi.org/10.1016/j.resconrec.2024.107498>, 2024.

1161 Liu, Z., Ciais, P., Deng, Z., Davis, S. J., Zheng, B., Wang, Y., Cui, D., Zhu, B., Dou,
1162 X., Ke, P., Sun, T., Guo, R., Zhong, H., Boucher, O., Bréon, F.-M., Lu, C., Guo,
1163 R., Xue, J., Boucher, E., Tanaka, K., and Chevallier, F.: Carbon Monitor, a
1164 near-real-time daily dataset of global CO₂ emission from fossil fuel and cement
1165 production, *Sci. Data*, 7, 392, <https://doi.org/10.1038/s41597-020-00708-7>,
1166 2020a.

1167 Liu, Z., Ciais, P., Deng, Z., Lei, R., Davis, S. J., Feng, S., Zheng, B., Cui, D., Dou, X.,
1168 Zhu, B., Guo, R., Ke, P., Sun, T., Lu, C., He, P., Wang, Y., Yue, X., Wang, Y., Lei,

1169 Y., Zhou, H., Cai, Z., Wu, Y., Guo, R., Han, T., Xue, J., Boucher, O., Boucher, E.,
1170 Chevallier, F., Tanaka, K., Wei, Y., Zhong, H., Kang, C., Zhang, N., Chen, B., Xi,
1171 F., Liu, M., Bréon, F.-M., Lu, Y., Zhang, Q., Guan, D., Gong, P., Kammen, D. M.,
1172 He, K., and Schellnhuber, H. J.: Near-real-time monitoring of global CO₂
1173 emissions reveals the effects of the COVID-19 pandemic, *Nat. Commun.*, 11,
1174 5172, <https://doi.org/10.1038/s41467-020-18922-7>, 2020b.

1175 Lv, Z., Wang, X., Deng, F., Ying, Q., Archibald, A. T., Jones, R. L., Ding, Y., Cheng,
1176 Y., Fu, M., Liu, Y., Man, H., Xue, Z., He, K., Hao, J., and Liu, H.: Source–
1177 Receptor Relationship Revealed by the Halted Traffic and Aggravated Haze in
1178 Beijing during the COVID-19 Lockdown, *Environ. Sci. Technol.*, 54,
1179 15660-15670, <https://doi.org/10.1021/acs.est.0c04941>, 2020.

1180 Ma, Q., Wang, J., Xiong, M., and Zhu, L.: Air Quality Index (AQI) Did Not Improve
1181 during the COVID-19 Lockdown in Shanghai, China, in 2022, Based on Ground
1182 and TROPOMI Observations, *Remote Sens.*, 15, 1295,
1183 <https://doi.org/10.3390/rs15051295>, 2023.

1184 Ministry of ecology and environment (MEE).: The list of technical specifications for
1185 the application and issuance of pollutant discharge permits issued by the ministry
1186 of ecology and environment, 2021.

1187 Ministry of ecology and environment (MEE).: Report on the State of the Ecology and
1188 Environment in China, 2022.

1189 MEIC: Multi-resolution Emission Inventory model for Climate and air pollution
1190 research, <http://meicmodel.org.cn/> (last visited on October 2025), 2024.

1191 National Bureau of Statistics of China (NBS): Statistical Yearbook of China, China
1192 Statistics Press, Beijing, 2023 (in Chinese).

1193 Requia, W. J., Di, Q., Silvern, R., Kelly, J. T., Koutrakis, P., Mickley, L. J., Sulprizio,
1194 M. P., Amini, H., Shi, L., and Schwartz, J.: An Ensemble Learning Approach for
1195 Estimating High Spatiotemporal Resolution of Ground-Level Ozone in the
1196 Contiguous United States, *Environ. Sci. Technol.*, 54, 11037-11047,
1197 <https://doi.org/10.1021/acs.est.0c01791>, 2020.

1198 State Council of the People’s Republic of China. Three-year Action Plan for

1199 Protecting Blue Sky. Central Government of the People's Republic of China
1200 (2018). http://www.gov.cn/zhengce/content/2018-07/03/content_5303158.htm.

1201 Schneider, R., Masselot, P., Vicedo-Cabrera, A. M., Sera, F., Blangiardo, M., Forlani,
1202 C., Douros, J., Jorba, O., Adani, M., Kouznetsov, R., Couvidat, F., Arteta, J.,
1203 Raux, B., Guevara, M., Colette, A., Barré, J., Peuch, V.-H., and Gasparrini, A.:
1204 Differential impact of government lockdown policies on reducing air pollution
1205 levels and related mortality in Europe, *Sci. Rep.*, 12, 726,
1206 <https://doi.org/10.1038/s41598-021-04277-6>, 2022.

1207 Shao, Y., Liu, R., Yang, J., Liu, M., Fang, W., Hu, L., Bi, J., and Ma, Z.: Economic
1208 Growth Facilitates Household Fuel Use Transition to Reduce PM_{2.5}-Related
1209 Deaths in China, *Environ. Sci. Technol.*, 57, 12663-12673,
1210 <https://doi.org/10.1021/acs.est.3c03276>, 2023.

1211 Shen, X., Kong, L., Shi, Y., Cao, X., Li, X., Wu, B., Zhang, H., and Yao, Z.:
1212 Multi-type Air Pollutant Emission Inventory of Non-road Mobile Sources in
1213 China for the Period 1990-2017, *Aerosol Air Qual. Res.*, 21, 210003,
1214 <https://doi.org/10.4209/aaqr.210003>, 2021.

1215 Shen, X., Che, H., Lv, T., Wu, B., Cao, X., Li, X., Zhang, H., Hao, X., Zhou, Q., and
1216 Yao, Z.: Real-world emission characteristics of
1217 semivolatile/intermediate-volatility organic compounds originating from nonroad
1218 construction machinery in the working process, *Sci. Total Environ.*, 858, 159970,
1219 <https://doi.org/10.1016/j.scitotenv.2022.159970>, 2023.

1220 Simayi, M., Shi, Y., Xi, Z., Ren, J., and Xie, S.: Emission trends of industrial VOCs in
1221 China since the clean air action and future reduction perspectives, *Sci. Total*
1222 *Environ.*, 826, 153994, <https://doi.org/10.1016/j.scitotenv.2022.153994>, 2022.

1223 Sokhi, R. S., Moussiopoulos, N., Baklanov, A., Bartzis, J., Coll, I., Finardi, S.,
1224 Friedrich, R., Geels, C., Grönholm, T., Halenka, T., Ketzel, M., Maragkidou, A.,
1225 Matthias, V., Moldanova, J., Ntziachristos, L., Schäfer, K., Suppan, P., Tsegas, G.,
1226 Carmichael, G., Franco, V., Hanna, S., Jalkanen, J.-P., Velders, G. J. M., and
1227 Kukkonen, J.: Advances in air quality research – current and emerging
1228 challenges, *Atmos. Chem. Phys.*, 22, 4615–4703,

1229 <https://doi.org/10.5194/acp-22-4615-2022>, 2022.

1230 Sun, S., Jin, J., Xia, M., Liu, Y., Gao, M., Zou, C., Wang, T., Lin, Y., Wu, L., Mao, H.,
1231 and Wang, P.: Vehicle emissions in a middle-sized city of China: Current status
1232 and future trends, *Environ. Int.*, 137, 105514,
1233 <https://doi.org/10.1016/j.envint.2020.105514>, 2020.

1234 State Council of the People's Republic of China. Three-year Action Plan for
1235 Protecting Blue Sky. Central People's Government of the People's Republic of
1236 China (2018).
1237 http://www.gov.cn/zhengce/content/2018-07/03/content_5303158.htm.

1238 Tang, L., Qu, J., Mi, Z., Bo, X., Chang, X., Anadon, L. D., Wang, S., Xue, X., Li, S.,
1239 Wang, X., and Zhao, X.: Substantial emission reductions from Chinese power
1240 plants after the introduction of ultra-low emissions standards, *Nat. Energy*, 4,
1241 929-938, <https://doi.org/10.1038/s41560-019-0468-1>, 2019.

1242 Tang, L., Ruan, J., Bo, X., Mi, Z., Wang, S., Dong, G., and Davis, S. J.: Plant-level
1243 real-time monitoring data reveal substantial abatement potential of air pollution
1244 and CO₂ in China's cement sector, *One Earth*, 5, 892-906,
1245 <https://doi.org/10.1016/j.oneear.2022.07.003>, 2022.

1246 Tong, D., Geng, G., Zhang, Q., Cheng, J., Qin, X., Hong, C., He, K., and Davis, S. J.:
1247 Health co-benefits of climate change mitigation depend on strategic power plant
1248 retirements and pollution controls, *Nat. Clim. Chang.*, 11, 1077-1083,
1249 <https://doi.org/10.1038/s41558-021-01216-1>, 2021.

1250 Wang, F., Li, Z., Zhang, K., Di, B., and Hu, B.: An overview of non-road equipment
1251 emissions in China, *Atmos. Environ.*, 132, 283-289,
1252 <https://doi.org/10.1016/j.atmosenv.2016.02.046>, 2016.

1253 Wang, H., He, Q., Kong, H., Qin, K., Zheng, B., Lin, J., and Zhao, Y.: Declining
1254 short-term emission control opportunity for major events in Chinese cities,
1255 *Nature Cities*, 2, 434-446, <https://doi.org/10.1038/s44284-025-00233-x>, 2025.

1256 Wang, K., Gao, J., Tian, H., Dan, M., Yue, T., Xue, Y., Zou, P., and Wang, C.: An
1257 emission inventory spatial allocate method based on POI data, *China Environ.*
1258 *Sci.*, 37, 2377-2382, <https://doi.org/10.13198/j.issn.1001-6929.2019.02.13>, 2017.

1259 (in Chinese).

1260 Wang, N., Xu, J., Pei, C., Tang, R., Zhou, D., Chen, Y., Li, M., Deng, X., Deng, T.,
1261 Huang, X., and Ding, A.: Air quality during COVID-19 lockdown in the Yangtze
1262 River Delta and the Pearl River Delta: Two different responsive mechanisms to
1263 emission reductions in China, *Environ. Sci. Technol.*, 55, 5721-5730,
1264 <https://doi.org/10.1021/acs.est.0c08383>, 2021.

1265 Wang, S. W., Zhang, Q., Streets, D. G., He, K. B., Martin, R. V., Lamsal, L. N., Chen,
1266 D., Lei, Y., and Lu, Z.: Growth in NO_x emissions from power plants in China:
1267 bottom-up estimates and satellite observations, *Atmos. Chem. Phys.*, 12, 4429–
1268 4447, <https://doi.org/10.5194/acp-12-4429-2012>, 2012.

1269 Wang, L., Liu, D., Yan, W., Kang, Z., Liu, R., Zhang, J., and Li, Z.: Spatio-temporal
1270 distribution, transport characteristics and synoptic patterns of ozone pollution
1271 near surface in Jiangsu province, China, *Atmos. Pollut. Res.*, 13, 101616,
1272 <https://doi.org/10.1016/j.apr.2022.101616>, 2022.

1273 Wang, Y., Zhao, Y., Liu, Y., Jiang, Y., Zheng, B., Xing, J., Liu, Y., Wang, S., and
1274 Nielsen, C. P.: Sustained emission reductions have restrained the ozone pollution
1275 over China, *Nat. Geosci.*, 16, 967-974,
1276 <https://doi.org/10.1038/s41561-023-01284-2>, 2023.

1277 Wei, X., Tong, Q., Magill, I., Vithaya, P., and Betz, R.: Evaluation of potential
1278 co-benefits of air pollution control and climate mitigation policies for China's
1279 electricity sector, <https://doi.org/10.1016/j.eneco.2020.104917>, 2020.

1280 Xiao, Q., Chang, H., Geng, G., and Liu, Y.: An Ensemble Machine-Learning Model
1281 To Predict Historical PM_{2.5} Concentrations in China from Satellite Data, *Environ.*
1282 *Sci. Technol.*, 52, 13260-13269, <https://doi.org/10.1021/acs.est.8b02917>, 2018.

1283 Xu, Y., Chen, S., Wang, Z., Liu, B., and Wang, L.: Multi-Scale Dynamics and Spatial
1284 Consistency of Economy and Population Based on NPP/VIIRS Nighttime Light
1285 Data and Population Imagery: A Case Study of the Yangtze River Delta, *Remote*
1286 *Sens.*, 16, 2806, <https://doi.org/10.3390/rs16152806>, 2024.

1287 Xu, R., Tong, D., Xiao, Q., Qin, X., Chen, C., Yan, L., Cheng, J., Cui, C., Hu, H., Liu,
1288 W., Yan, X., Wang, H., Liu, X., Geng, G., Lei, Y., Guan, D., He, K., and Zhang,

1289 Q. MEIC-global-CO₂: A new global CO₂ emission inventory with
1290 highly-resolved source category and sub-country information, *Sci. China Earth*
1291 *Sci.*, 66, doi: <https://doi.org/10.1007/s11430-023-1230-3>, 2023.

1292 Yang, X. F., Liu, H., Man, H. Y., and He, K. B.: Characterization of road freight
1293 transportation and its impact on the national emission inventory in China, *Atmos.*
1294 *Chem. Phys.*, 15, 2105–2118, <https://doi.org/10.5194/acp-15-2105-2015>, 2015.

1295 Yang, D., Zhang, S., Niu, T., Wang, Y., Xu, H., Zhang, K. M., and Wu, Y.:
1296 High-resolution mapping of vehicle emissions of atmospheric pollutants based
1297 on large-scale, real-world traffic datasets, *Atmos. Chem. Phys.*, 19, 8831–8843,
1298 <https://doi.org/10.5194/acp-19-8831-2019>, 2019.

1299 Yang, L., Hu, Y.-J., Wang, H., Li, C., Tang, B.-J., Wang, B., and Cui, H.: Uncertainty
1300 quantification of CO₂ emissions from China's civil aviation industry to 2050,
1301 *J. Environ. Manage.*, 336, 117624,
1302 <https://doi.org/10.1016/j.jenvman.2023.117624>, 2023.

1303 Yun, X., Meng, W., Xu, H., Zhang, W., Yu, X., Shen, H., Chen, Y., Shen, G., Ma, J., Li,
1304 B., Cheng, H., Hu, J., and Tao, S.: Coal Is Dirty, but Where It Is Burned
1305 Especially Matters, *Environ. Sci. Technol.*, 55, 7316-7326,
1306 <https://doi.org/10.1021/acs.est.1c01148>, 2021.

1307 Zhan, Y., Xie, M., Zhao, W., Wang, T., Gao, D., Chen, P., Tian, J., Zhu, K., Li, S.,
1308 Zhuang, B., Li, M., Luo, Y., and Zhao, R.: Quantifying the seasonal variations in
1309 and regional transport of PM_{2.5} in the Yangtze River Delta region, China:
1310 characteristics, sources, and health risks, *Atmos. Chem. Phys.*, 23, 9837–9852,
1311 <https://doi.org/10.5194/acp-23-9837-2023>, 2023.

1312 Zhang, B., Zhang, J., and Feng, T.: A global comparative study on the impact of
1313 COVID-19 policy on atmospheric nitrogen dioxide (NO₂): Evidence from remote
1314 sensing data in 2019–2022, *J. Environ. Manage.*, 367, 121851,
1315 <https://doi.org/10.1016/j.jenvman.2024.121851>, 2024.

1316 Zhang, Q., Zheng, Y., Tong, D., Shao, M., Wang, S., Zhang, Y., Xu, X., Wang, J., He,
1317 H., Liu, W., Ding, Y., Lei, Y., Li, J., Wang, Z., Zhang, X., Wang, Y., Cheng, J.,
1318 Liu, Y., Shi, Q., Yan, L., Geng, G., Hong, C., Li, M., Liu, F., Zheng, B., Cao, J.,

1319 Ding, A., Gao, J., Fu, Q., Huo, J., Liu, B., Liu, Z., Yang, F., He, K., and Hao, J.:
1320 Drivers of improved PM_{2.5} air quality in China from 2013 to 2017, *Proc. Natl.*
1321 *Acad. Sci.*, 116, 24463-24469, <https://doi.org/10.1073/pnas.1907956116>, 2019.

1322 Zhang, S., Zhang, C., Cai, W., Bai, Y., Callaghan, M., Chang, N., Chen, B., Chen, H.,
1323 Cheng, L., Dai, H., Dai, X., Fan, W., Fang, X., Gao, T., Geng, Y., Guan, D., Hu,
1324 Y., Hua, J., Huang, C., Huang, H., Huang, J., Huang, X., Ji, J. S., Jiang, Q., Jiang,
1325 X., Kieser, G., Li, T., Liang, L., Lin, B., Lin, H., Liu, H., Liu, Q., Liu, X., Liu, Z.,
1326 Liu, Z., Liu, Y., Lu, B., Lu, C., Luo, Z., Ma, W., Mi, Z., Ren, C., Romanello, M.,
1327 Shen, J., Su, J., Sun, Y., Sun, X., Tang, X., Walawender, M., Wang, C., Wang, Q.,
1328 Wang, R., Warnecke, L., Wei, W., Wen, S., Xie, Y., Xiong, H., Xu, B., Yan, Y.,
1329 Yang, X., Yao, F., Yu, L., Yuan, J., Zeng, Y., Zhang, J., Zhang, L., Zhang, R.,
1330 Zhang, S., Zhang, S., Zhao, M., Zheng, D., Zhou, H., Zhou, J., Zhou, Z., Luo, Y.,
1331 and Gong, P.: The 2023 China report of the Lancet Countdown on health and
1332 climate change: taking stock for a thriving future, *The Lancet Public Health*, 8,
1333 e978-e995, [https://doi.org/10.1016/S2468-2667\(23\)00245-1](https://doi.org/10.1016/S2468-2667(23)00245-1), 2023.

1334 Zhang, Y., Yang, X., Brown, R., Yang, L., Morawska, L., Ristovski, Z., Fu, Q., and
1335 Huang, C.: Shipping emissions and their impacts on air quality in China, *Sci.*
1336 *Total Environ.*, 581, 186-198, <https://doi.org/10.1016/j.scitotenv.2016.12.098>,
1337 2017.

1338 Zhang, Y., Bo, X., Zhao, Y., and Nielsen, C. P.: Benefits of current and future policies
1339 on emissions of China's coal-fired power sector indicated by continuous emission
1340 monitoring, *Environ. Pollut.*, 251, 415-424,
1341 <https://doi.org/10.1016/j.envpol.2019.05.021>, 2019.

1342 Zhao, Y., Wang, S., Nielsen, C. P., Li, X., and Hao, J.: Establishment of a database of
1343 emission factors for atmospheric pollutants from Chinese coal-fired power plants,
1344 *Atmos. Environ.*, 44, 1515-1523, <https://doi.org/10.1016/j.atmosenv.2010.01.017>,
1345 2010.

1346 Zhao, Y., Zhang, J., and Nielsen, C. P.: The effects of recent control policies on trends
1347 in emissions of anthropogenic atmospheric pollutants and CO₂ in China, *Atmos.*
1348 *Chem. Phys.*, 13, 487-508, <https://doi.org/10.5194/acp-13-487-2013>, 2013.

1349 Zhao, Y., Zhang, K., Xu, X., Shen, H., Zhu, X., Zhang, Y., Hu, Y., and Shen, G.:
1350 Substantial Changes in Nitrogen Dioxide and Ozone after Excluding
1351 Meteorological Impacts during the COVID-19 Outbreak in Mainland China,
1352 *Environ. Sci. Technol. Lett.*, **7**, 402–408,
1353 <https://doi.org/10.1021/acs.estlett.0c00304>, 2020a.

1354 Zhao, Y., Yuan, M., Huang, X., Chen, F., and Zhang, J.: Quantification and evaluation
1355 of atmospheric ammonia emissions with different methods: a case study for the
1356 Yangtze River Delta region, China, *Atmos. Chem. Phys.*, **20**, 4275–4294,
1357 <https://doi.org/10.5194/acp-20-4275-2020>, 2020b.

1358 Zhao, S., Hu, B., Liu, H., Du, C., Xia, X., and Wang, Y.: The influence of aerosols on
1359 the NO₂ photolysis rate in a suburban site in North China, *Sci. Total Environ.*,
1360 144788, <https://doi.org/10.1016/j.scitotenv.2020.144788>, 2021.

1361 Zhao, Y., Xi, M., Zhang, Q., Dong, Z., Ma, M., Zhou, K., Xu, W., Xing, J., Zheng, B.,
1362 Wen, Z., Liu, X., Nielsen, C. P., Liu, Y., Pan, Y., and Zhang, L.: Decline in bulk
1363 deposition of air pollutants in China lags behind reductions in emissions, *Nat.*
1364 *Geosci.*, **15**, 190–195, <https://doi.org/10.1038/s41561-022-00899-1>, 2022.

1365 Zhao, X., Shao, B., Su, J., and Tian, N.: Exploring synergistic evolution of carbon
1366 emissions and air pollutants and spatiotemporal heterogeneity of influencing
1367 factors in Chinese cities, *Sci. Rep.*, **15**, 2657,
1368 <https://doi.org/10.1038/s41598-024-84212-7>, 2025.

1369 Zheng, B., Tong, D., Li, M., Liu, F., Hong, C., Geng, G., Li, H., Li, X., Peng, L., Qi, J.,
1370 Yan, L., Zhang, Y., Zhao, H., Zheng, Y., He, K., and Zhang, Q.: Trends in China's
1371 anthropogenic emissions since 2010 as the consequence of clean air actions,
1372 *Atmos. Chem. Phys.*, **18**, 14095–14111,
1373 <https://doi.org/10.5194/acp-18-14095-2018>, 2018.

1374 Zheng, B., G. Geng, P. Ciais, S. J. Davis, R. V. Martin, J. Meng, N. Wu, F. Chevallier,
1375 G. Broquet, F. Boersma, R. J. van der A, J. Lin, D. Guan, Y. Lei, K. He, Q.
1376 Zhang. Satellite-based estimates of decline and rebound in China's CO₂
1377 emissions during COVID-19 pandemic. *Sci. Adv.*, **6**, eabd4998,
1378 <https://doi.org/10.1126/sciadv.abd4998>, 2020.

- 1379 Zheng, B., Zhang, Q., Geng, G., Chen, C., Shi, Q., Cui, M., Lei, Y., and He, K.:
1380 Changes in China's anthropogenic emissions and air quality during the
1381 COVID-19 pandemic in 2020, *Earth Syst. Sci. Data*, 13, 2895–2907,
1382 <https://doi.org/10.5194/essd-13-2895-2021>, 2021.
- 1383 Zhou, Y., Zhao, Y., Mao, P., Zhang, Q., Zhang, J., Qiu, L., and Yang, Y.: Development
1384 of a high-resolution emission inventory and its evaluation and application
1385 through air quality modeling for Jiangsu Province, China, *Atmos. Chem. Phys.*,
1386 17, 211–233, <https://doi.org/10.5194/acp-17-211-2017>, 2017.
- 1387 Zhou, Z., Tan, Q., Liu, H., Deng, Y., Wu, K., Lu, C., and Zhou, X.: Emission
1388 characteristics and high-resolution spatial and temporal distribution of pollutants
1389 from motor vehicles in Chengdu, China, *Atmos. Pollut. Res.*, 10, 749-758,
1390 <https://doi.org/10.1016/j.apr.2018.12.002>, 2019.
- 1391 Zhou, K., Xu, W., Zhang, L., Ma, M., Liu, X., and Zhao, Y.: Estimating nitrogen and
1392 sulfur deposition across China during 2005 to 2020 based on multiple statistical
1393 models, *Atmos. Chem. Phys.*, 23, 8531–8551,
1394 <https://doi.org/10.5194/acp-23-8531-2023>, 2023.

1395

1396 **Figure captions**

1397 **Figure 1** The research framework of near-real-time emission estimation and
1398 application in this work.

1399 **Figure 2** Daily emission estimates of anthropogenic air pollutants by sector for
1400 Jiangsu Province in 2022. (a) NO_x; (b) SO₂; (c) PM_{2.5}; (d) NMVOCs; (e) NH₃.

1401 **Figure 3** Spatial distribution of anthropogenic NO_x emissions for Jiangsu Province in
1402 2022 with a horizontal resolution of 3 × 3 km. (a) Total emissions; (b) Power; (c)
1403 Industry; (d) Vehicle; (e) Off-road transportation; (f) Residential. The map data
1404 provided by Resource and Environment Data Cloud Platform are freely available for
1405 academic use (<http://www.resdc.cn/data.aspx?DATAID=201>), © Institute of
1406 Geographic Sciences & Natural Resources Research, Chinese Academy of Sciences.

1407 **Figure 4** The monthly air pollutant emissions for Jiangsu Province in 2022 estimated
1408 in this study (a, c, and e) and in national emission inventory (MEIC; b, d, and f). The
1409 emissions of SO₂ (a and b), NO_x (c and d) and primary PM_{2.5} (e and f) are contained.
1410 The red lines with triangles represent the observed monthly surface concentrations of
1411 corresponding air pollutants.

1412 **Figure 5** The differences between the emissions of NO_x (a), SO₂ (b), PM_{2.5} (c) and
1413 NMVOCs (d) in April-May for 2022 and 2023 in Jiangsu Province. The first column
1414 illustrates the daily total emissions and the differences for the period of the two years.
1415 The second column illustrates the contributions of various source categories to the
1416 differences in daily total emissions, and the third column aggregates them for the
1417 whole period.

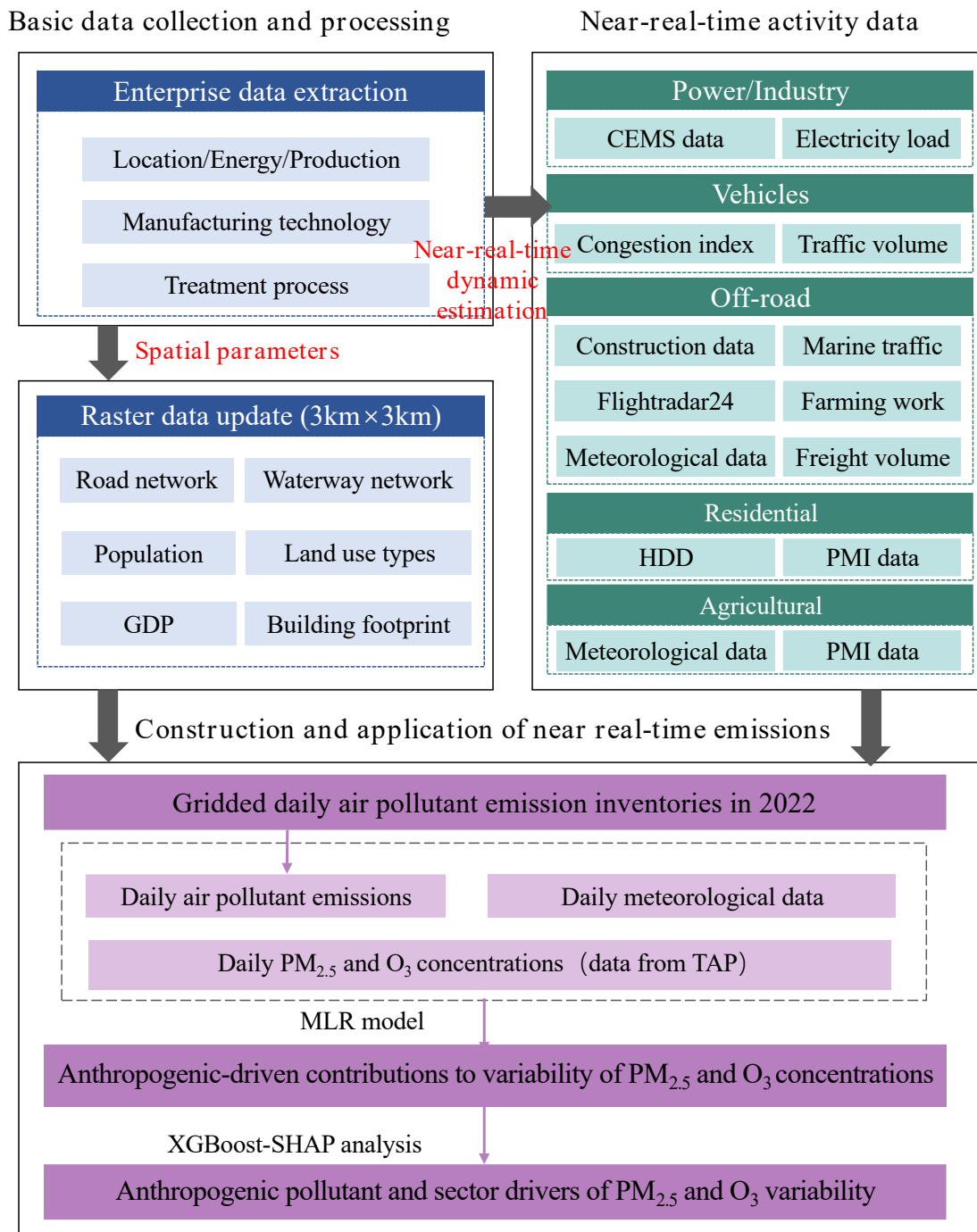
1418 **Figure 6** Comparison between the observed daily PM_{2.5} concentrations (blue lines)
1419 and the simulated concentrations with different emission inventories in Jiangsu
1420 Province for January (a), April (b), July (c), and October (d) in 2022. The simulations
1421 were conducted using the near-real-time emission inventory developed in this work
1422 (red lines) and the revised national emission inventory MEIC (MEIC-revision, black
1423 lines). See Section 2.3 for the rationale of MEIC revision.

1424 **Figure 7** Comparison between the observed daily maximum 8-hour average (MDA8)
1425 O₃ concentrations and the simulated concentrations with different emission
1426 inventories in Jiangsu Province for January (a), April (b), July (c), and October (d) in
1427 2022. The simulations were conducted using the near-real-time emission inventory
1428 developed in this work (red lines) and the revised national emission inventory MEIC
1429 (MEIC-revision, black lines). See Section 2.3 for the rationale of MEIC revision.

1430 **Figure 8** The monthly anomaly in PM_{2.5} (a) and MDA8 O₃ concentrations (b) driven
1431 by the changing daily emissions for Jiangsu Province in 2022, based on the MLR
1432 model.

1433 **Figure 9** Anthropogenic pollutant and sector drivers of PM_{2.5} and MDA8 O₃
1434 variability. (a) and (b) illustrate the contributions of pollutant-sector combinations to

1435 the variability of PM_{2.5} in January and that of O₃ in July, derived from SHAP analysis.
 1436 The black dashed lines represent the observed daily ground-level concentrations of
 1437 PM_{2.5} and MDA8 O₃. (c) and (d) provided the contributions of the changing emissions
 1438 from different sectors, with those of various precursor species aggregated.



1439

1440 **Figure 1** The research framework of near-real-time emission estimation and
 1441 application in this work.

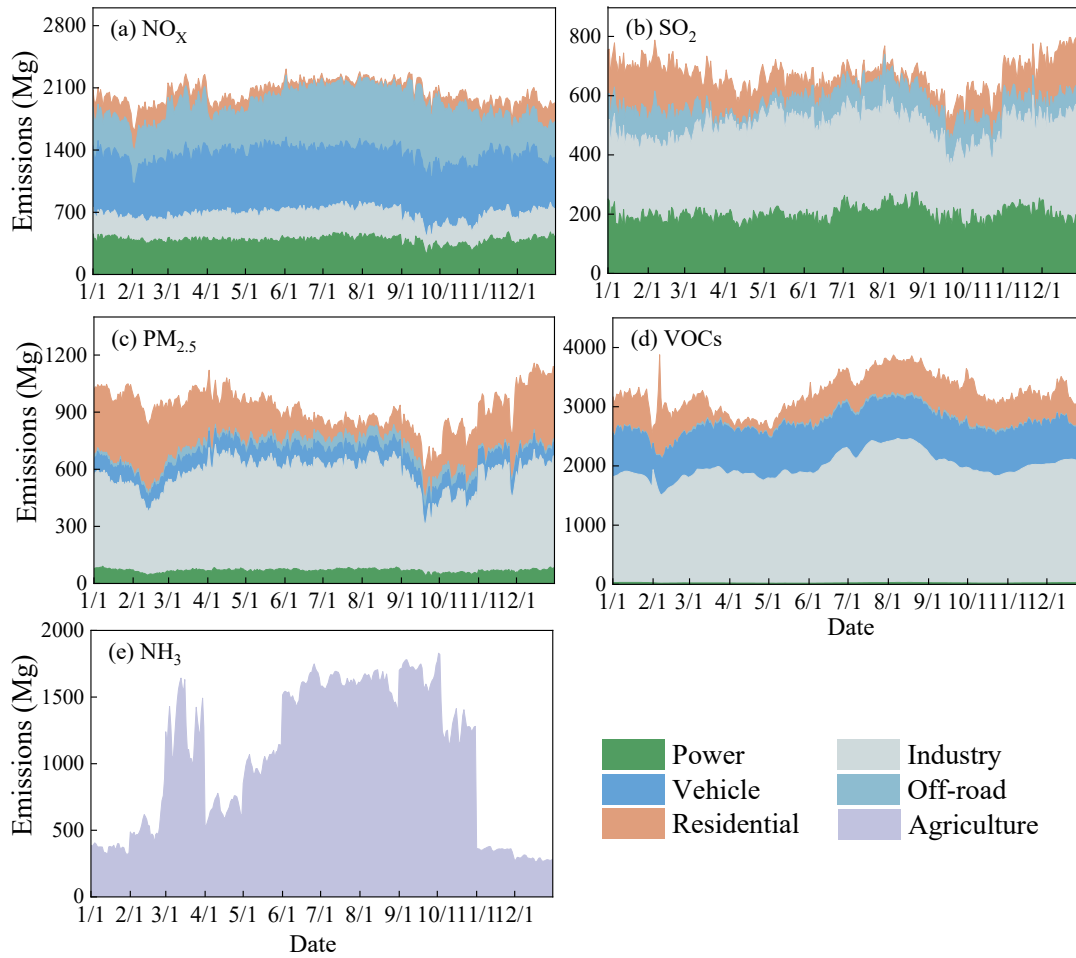


Figure 2 Daily emission estimates of anthropogenic air pollutants by sector for Jiangsu Province in 2022. (a) NO_x ; (b) SO_2 ; (c) $\text{PM}_{2.5}$; (d) NMVOCs; (e) NH_3 .

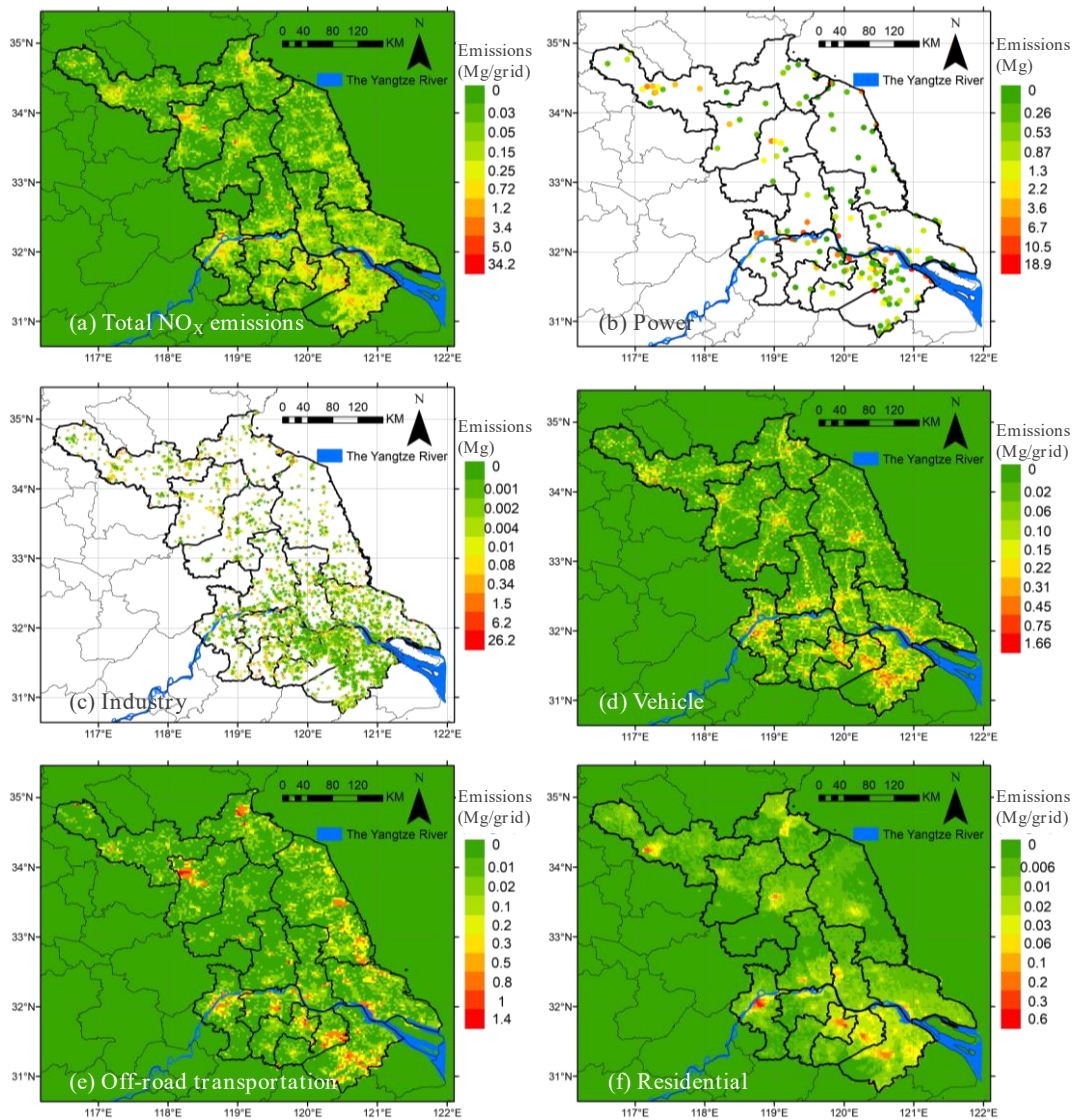


Figure 3 Spatial distribution of anthropogenic NO_x emissions for Jiangsu Province in 2022 with a horizontal resolution of 3×3 km. (a) Total emissions; (b) Power; (c) Industry; (d) Vehicle; (e) Off-road transportation; (f) Residential. The map data provided by Resource and Environment Data Cloud Platform are freely available for academic use (<http://www.resdc.cn/data.aspx?DATAID=201>), © Institute of Geographic Sciences & Natural Resources Research, Chinese Academy of Sciences.

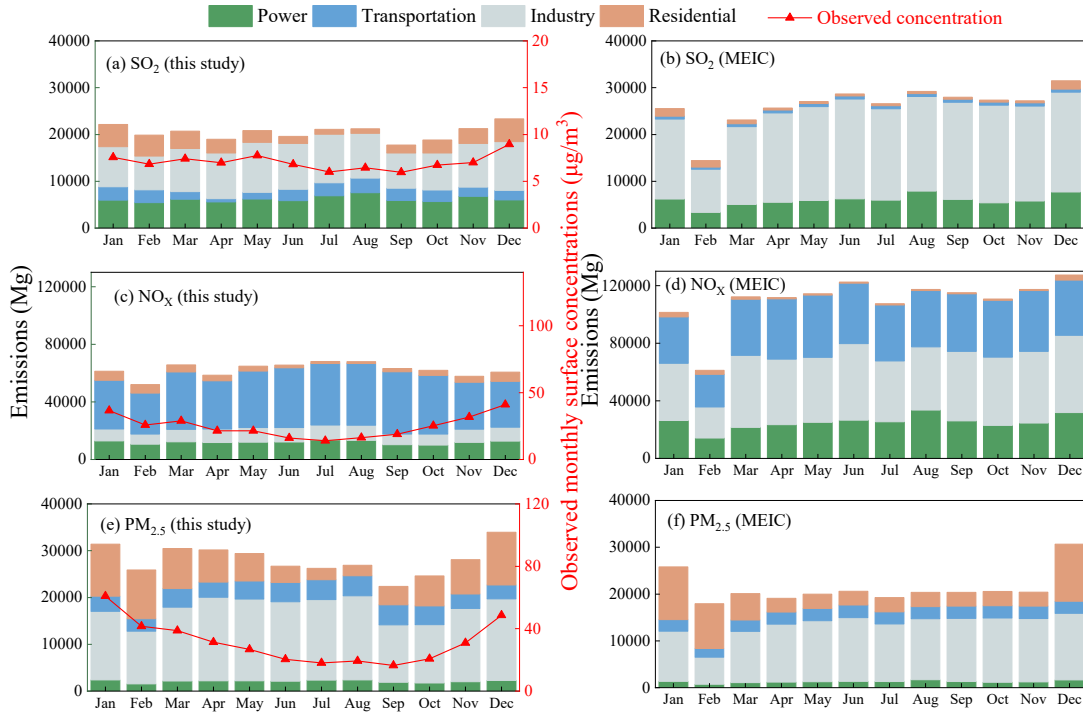


Figure 4 The monthly air pollutant emissions for Jiangsu Province in 2022 estimated in this study (a, c, and e) and in national emission inventory (MEIC; b, d, and f). The emissions of SO₂ (a and b), NO_x (c and d) and primary PM_{2.5} (e and f) are contained. The red lines with triangles represent the observed monthly surface concentrations of corresponding air pollutants.

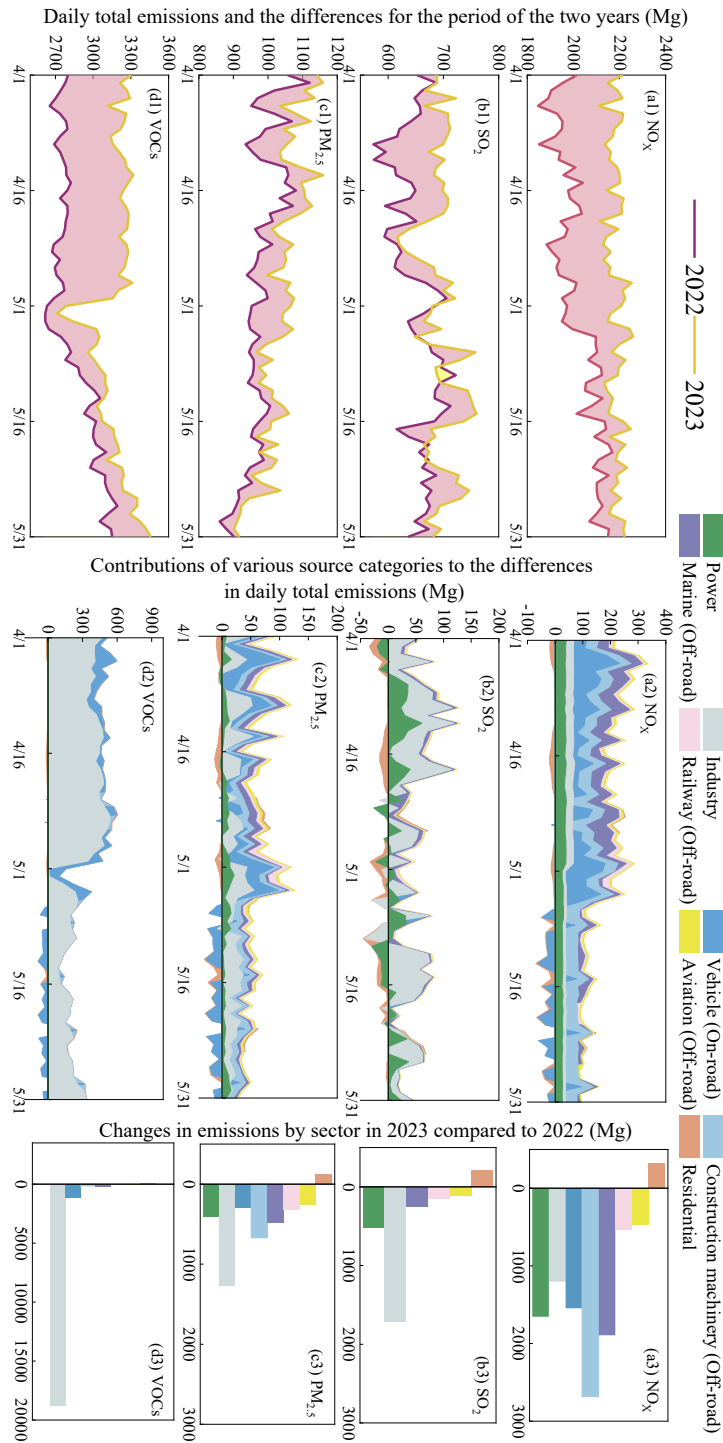


Figure 5 The differences between the emissions of NO_x (a), SO₂ (b), PM_{2.5} (c) and NMVOCs (d) in April-May for 2022 and 2023 in Jiangsu Province. The first column illustrates the daily total emissions and the differences for the period of the two years. The second column illustrates the contributions of various source categories to the differences in daily total emissions, and the third column aggregates them for the whole period.

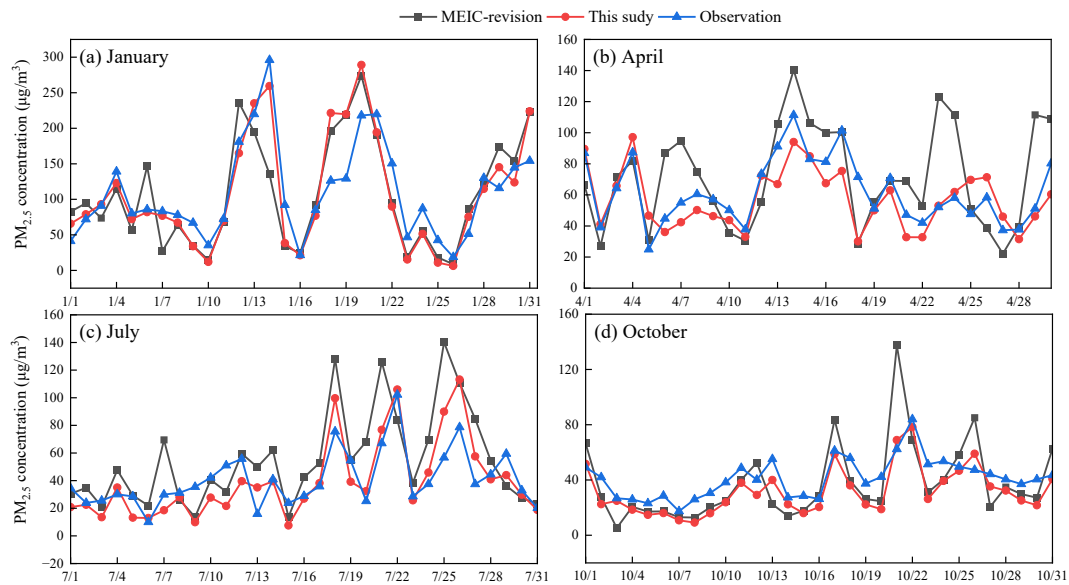


Figure 6 Comparison between the observed daily $PM_{2.5}$ concentrations (blue lines) and the simulated concentrations with different emission inventories in Jiangsu Province for January (a), April (b), July (c), and October (d) in 2022. The simulations were conducted using the near-real-time emission inventory developed in this work (red lines) and the revised national emission inventory MEIC (MEIC-revision, black lines). See Section 2.3 for the rationale of MEIC revision.

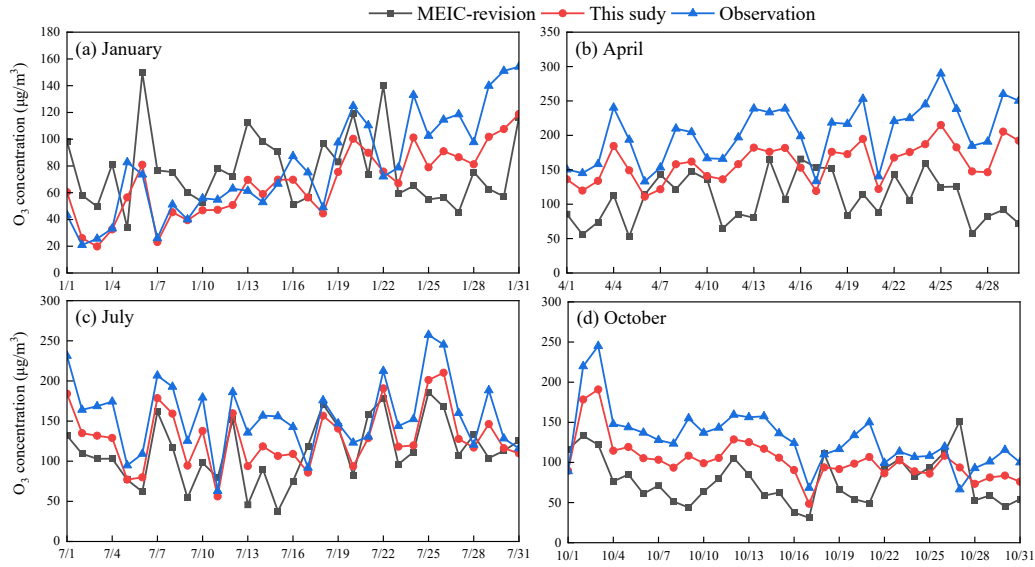


Figure 7 Comparison between the observed daily maximum 8-hour average (MDA8) O₃ concentrations and the simulated concentrations with different emission inventories in Jiangsu Province for January (a), April (b), July (c), and October (d) in 2022. The simulations were conducted using the near-real-time emission inventory developed in this work (red lines) and the revised national emission inventory MEIC (MEIC-revision, black lines). See Section 2.3 for the rationale of MEIC revision.

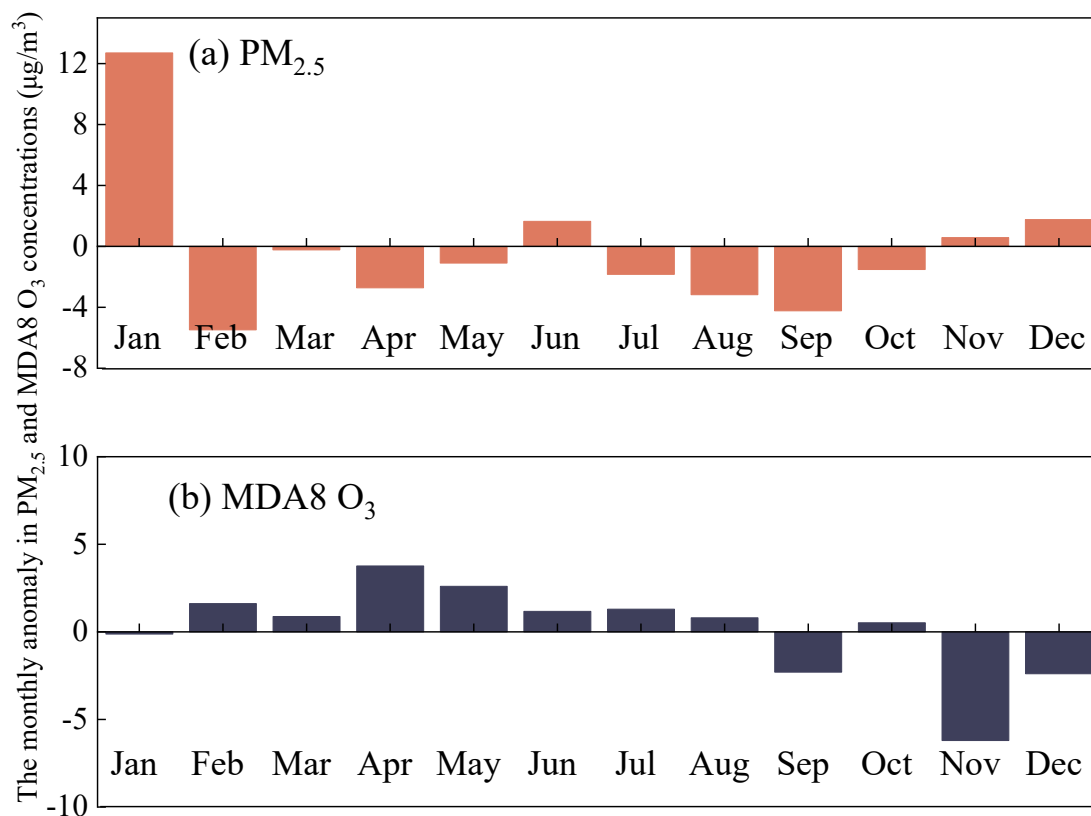


Figure 8 The monthly anomaly in $PM_{2.5}$ (a) and MDA8 O_3 concentrations (b) driven by the changing daily emissions for Jiangsu Province in 2022, based on the MLR model.

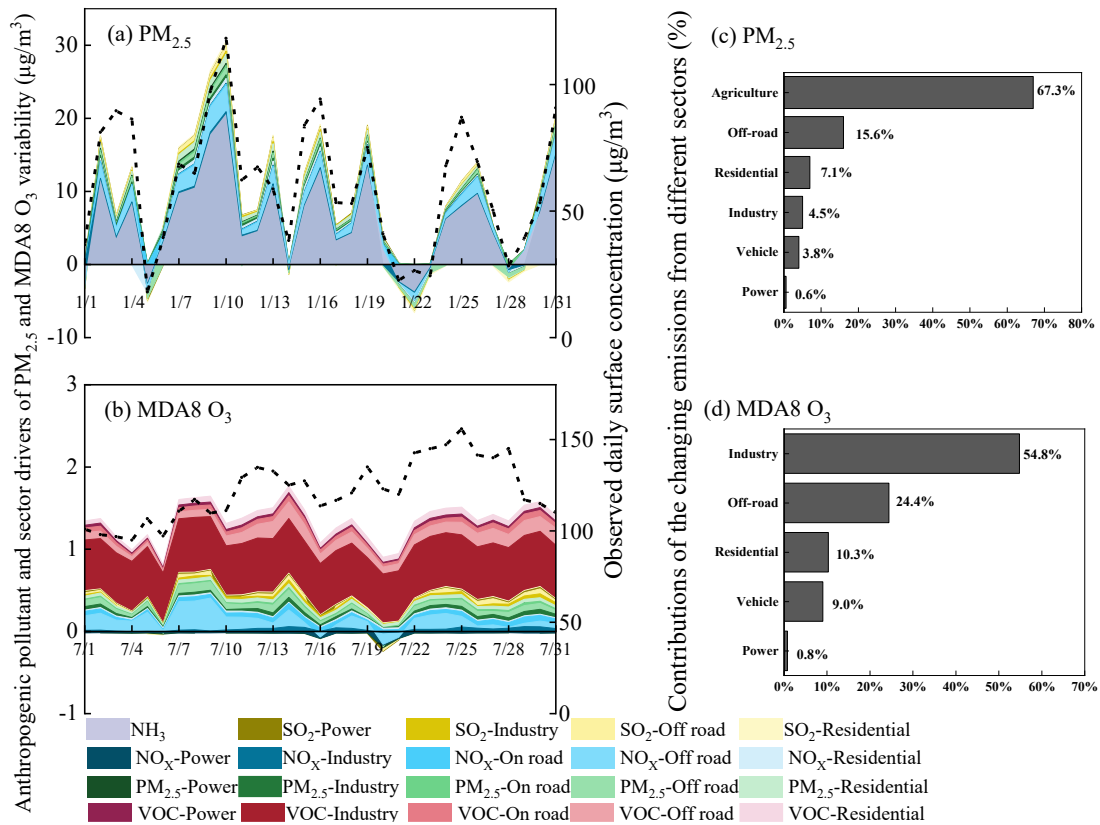


Figure 9 Anthropogenic pollutant and sector drivers of $PM_{2.5}$ and MDA8 O_3 variability. (a) and (b) illustrate the contributions of pollutant-sector combinations to the variability of $PM_{2.5}$ in January and that of O_3 in July, derived from SHAP analysis. The black dashed lines represent the observed daily ground-level concentrations of $PM_{2.5}$ and MDA8 O_3 . (c) and (d) provided the contributions of the changing emissions from different sectors, with those of various precursor species aggregated.